Inhibition of chemotherapy resistant breast cancer stem cells by a ROR1 specific antibody

Suping Zhang[a,b,1], Han Zhang[b,1], Emanuela M. Ghia[b,1], Jiajia Huang[c], Liufeng Wu[a], Jianchao Zhang[a], Sharon Lam[b], Yang Lei[a], Jinsong He[d], Bing Cui[b], George F. Widhopf II[b], Jian Yu[b], Richard Schwab[b], Karen Messer[b,e], Wenqi Jiang[c], Barbara A. Parker[b], Dennis A. Carson[a,b,2], and Thomas J. Kipps[a,b,2]

[a]Guangdong Key Laboratory for Genome Stability and Human Disease Prevention, Department of Pharmacology, International Cancer Center, Shenzhen University Health Science Center, 518060 Shenzhen, China; [b]Moores Cancer Center, University of California, San Diego, La Jolla, CA 92093; [c]State Key Laboratory of Oncology in South China, Department of Medical Oncology, Collaborative Innovation Center for Cancer Medicine, Sun Yat-sen University Cancer Center, 510060 Guangzhou, China; [d]Department of Breast Surgery, The Peking University Shenzhen Hospital, 518036 Shenzhen, China; and [e]Division of Biostatistics and Bioinformatics, Department of Family Medicine and Public Health, University of California, San Diego, La Jolla, CA 92093

Contributed by Dennis A. Carson, November 9, 2018 (sent for review September 26, 2018; reviewed by Caroline Ford and Kay Huebner)

Breast cancers enduring treatment with chemotherapy may be enriched for cancer stem cells or tumor-initiating cells, which have an enhanced capacity for self-renewal, tumor initiation, and/or metastasis. Breast cancer cells that express the type I tyrosine kinaselike orphan receptor ROR1 also may have such features. Here we find that the expression of ROR1 increased in breast cancer cells following treatment with chemotherapy, which also enhanced expression of genes induced by the activation of Rho-GTPases, Hippo-YAP/TAZ, or B lymphoma Mo-MLV insertion region 1 homolog (BMI1). Expression of ROR1 also enhanced the capacity of breast cancer cells to invade Matrigel, form spheroids, engraft in Rag2$^{-/-}\gamma_c^{-/-}$ mice, or survive treatment with paclitaxel. Treatment of mice bearing breast cancer patient-derived xenografts (PDXs) with the humanized anti-ROR1 monoclonal antibody cirmtuzumab repressed expression of genes associated with breast cancer stemness, reduced activation of Rho-GTPases, Hippo-YAP/TAZ, or BMI1, and impaired the capacity of breast cancer PDXs to metastasize or reengraft Rag2$^{-/-}\gamma_c^{-/-}$ mice. Finally, treatment of PDX-bearing mice with cirmtuzumab and paclitaxel was more effective than treatment with either alone in eradicating breast cancer PDXs. These results indicate that targeting ROR1 may improve the response to chemotherapy of patients with breast cancer.

breast-cancer stem cells | chemotherapy | ROR1 | ROR1-signaling | cirmtuzumab

Breast cancers enduring chemotherapy may be enriched for cells with mesenchymal or stemness features, which can enable metastases or tumor relapse (1, 2). Epithelial cancer cells that possess or acquire a mesenchymal phenotype have an enhanced capacity for migration and invasion, a process known as epithelial-to-mesenchymal transition (EMT). In addition, EMT-master-transcription factors (e.g., SNAI1) can enhance the tumor-initiation capacity of cancer cells (3, 4). Cancer cells with the capacity to regrow the tumor are called tumor-initiation cells or cancer stem cells (CSCs); such cells have the capacity to self-renew and/or differentiate and thereby repopulate the primary tumor or establish metastatic tumors at distant sites (5). Recent studies demonstrate that cancer cells may acquire stemness features of CSCs in response to signals derived from the tumor microenvironment and/or following treatment with chemotherapy (5). If so, then targeting the CSC pathways that induce EMT and/or that account for the acquisition of tumor *stemness* may be more effective than strategies that only target existent CSCs (6).

CSCs with stemness features have the distinctive capacity to form nonadherent cellular spheroids or engraft immune-deficient mice (1, 7). Such cells have gene-expression signatures that reflect their relatively high capacity for self-renewal and ability to regenerate the entire tumor population (1). Notable is the expression of B lymphoma Mo-MLV insertion region 1 homolog (BMI1), a transcription repressor that belongs to the polycomb-group family of proteins; high-level expression of BMI1 is associated with breast cancers that have a basal-like phenotype, which typically is associated with relatively poor survival (8). BMI1 promotes self-renewal and the acquisition of a tumor-initiation capacity associated with CSCs (9–13). Moreover, BMI1 can promote expression of genes encoding ATP-binding cassette transporters, which can enhance resistance to chemotherapy (3, 11).

Associated with cancer stemness is ROR1 (14), a type I tyrosine kinaselike orphan receptor, which is expressed by many cancers but not by normal postpartum tissues (15, 16). Prior studies found that breast cancers with high levels of ROR1 typically were poorly differentiated and expressed markers associated with EMT (15, 17). High-level breast cancer-cell expression of ROR1 associates with a relatively rapid relapse after therapy and short survival (15, 17, 18). On the other hand, silencing *ROR1* could repress the expression of genes associated with EMT and/or impair cancer-cell migration/invasion and metastasis, indicating that ROR1 may play a role in inducing stemness of breast cancer cells (17).

ROR1 can serve as a receptor for Wnt5a (19), which may be expressed by tumor cells or by accessory cells within tumor microenvironment (20, 21). Wnt5a can induce noncanonical Wnt signaling in chronic lymphocytic leukemia (CLL), leading to activation of Rho-GTPases and enhanced tumor-cell migration,

Significance

We report that breast cancer cells surviving treatment with paclitaxel express relatively high levels of ROR1, which can induce activation of stem-cell signaling pathways in response to Wnt5a. A humanized anti-ROR1 drug, cirmtuzumab, can inhibit ROR1-dependent activation of such signaling and impair the capacity of post-treatment breast cancer cells to metastasize or reengraft immune-deficient mice.

Author contributions: S.Z., H.Z., E.M.G., B.A.P., and T.J.K. designed research; S.Z., H.Z., L.W., J.Z., S.L., Y.L., B.C., and J.Y. performed research; J. Huang, J. He, G.F.W., R.S., and W.J. contributed new reagents/analytic tools; S.Z., H.Z., E.M.G., L.W., J.Z., K.M., and T.J.K. analyzed data; and S.Z., H.Z., E.M.G., B.A.P., D.A.C., and T.J.K. wrote the paper.

Reviewers: C.F., University of New South Wales; and K.H., Ohio State University Comprehensive Cancer Center.

Conflict of interest statement: Cirmtuzumab was developed by T.J.K. in the T.J.K. laboratory and licensed by the University of California to Onternal Therapeutics, Inc., which provided stock options and research funding to the T.K.J. laboratory.

Data deposition: Raw sequencing files have been deposited in the Gene Expression Omnibus (GEO) database, https://www.ncbi.nlm.nih.gov/geo (accession no. GSE108632).

[1]S.Z., H.Z., and E.M.G. contributed equally to this work.

[2]To whom correspondence may be addressed. Email: dcarson@ucsd.edu or tkipps@ucsd.edu.

This article contains supporting information online at www.pnas.org/lookup/suppl/doi:10.1073/pnas.1816262116/-/DCSupplemental.

proliferation, and survival (22). Rho proteins, including RhoA, Rac1, and cdc42, are expressed at high levels in breast cancer cells relative to non-neoplastic cells of normal breast tissue (23). Activation of Rho-GTPases can contribute to oncogenesis and enhance the resistance to chemotherapy (24). In addition, activation of Rho-GTPases may induce Hippo-YAP/TAZ, which helps maintain the stemness of embryonic or induced-pluripotent stem cells and can promote the invasiveness, cytotoxic-drug resistance, and the metastatic potential of cancer cells (25–29). However, lacking is evidence that targeting ROR1 can repress breast CSCs or inhibit the acquisition of stemness features by breast cancer cells persisting after chemotherapy.

We examined for the expression of ROR1 in human breast cancer cells of patients or mice engrafted with breast cancer patient-derived xenografts (PDXs) before and after treatment with chemotherapy. In addition, we examined whether the humanized anti-ROR1 monoclonal antibody (mAb) cirmtuzumab could block Wnt5a-induced ROR1 signaling and thereby manifest antitumor activity alone or in combination with paclitaxel in mice bearing breast cancer PDXs.

Results

Breast Cancer Tissues After Chemotherapy Are Enriched for ROR1^{+} Cells. We obtained formalin-fixed paraffin-embedded biopsy material from patients ($n = 22$) with invasive ductal breast adenocarcinoma before (pre) and after (post) neoadjuvant chemotherapy, consisting of four to six cycles of a combination of docetaxel, doxorubicin or epirubicin, and/or cyclophosphamide. We examined for the expression of ROR1 via immunohistochemistry (Fig. 1*A* and *SI Appendix*, Fig. S1*A*). Consistent with our previous findings (15), ROR1 was detected on either estrogen receptor-positive (ER^{+}) or ER-negative (ER^{-}) breast cancer cells. Here, we found breast cancer expression of ROR1 increased in 14 (64%) of 22-matched specimens, including ER^{+} or ER^{-} breast cancer specimens. The intensity of staining for ROR1 did not change with therapy in seven (32%) cases (Fig. 1*A* and *SI Appendix*, Table S1). Only one post-treatment specimen had a lower expression of ROR1 compared with the matched pretreatment sample (*SI Appendix*, Table S1).

ROR1^{Hi} Breast Cancer Cells Have Stemness Characteristics. To examine the relevance of ROR1 in breast cancer, we established breast cancer PDXs in Rag2$^{-/-}\gamma_c^{-/-}$ mice (*SI Appendix*, Table S2). The PDXs retained the heterogeneity commonly found in primary tumors, which typically have small proportions of cells with stemness features. For example, only 0.6% or 6.5% of the tumor cells in PDX1 or PDX4, respectively, had detectable aldehyde dehydrogenase 1 (ALDH1) enzymatic activity, a commonly used marker of CSCs (*SI Appendix*, Table S2) (30). Breast cancer PDX cells with features of CSCs, such as the demonstration of ALDH1-enzymatic activity (ALDH1^{+}) or expression of CD44 with low-level CD24 (CD44^{+}/CD24^{Low} cells), had higher levels of ROR1 than PDX cells of the same tumor lacking such CSC characteristics, e.g., cells that were ALDH1^{Neg} or that expressed high levels

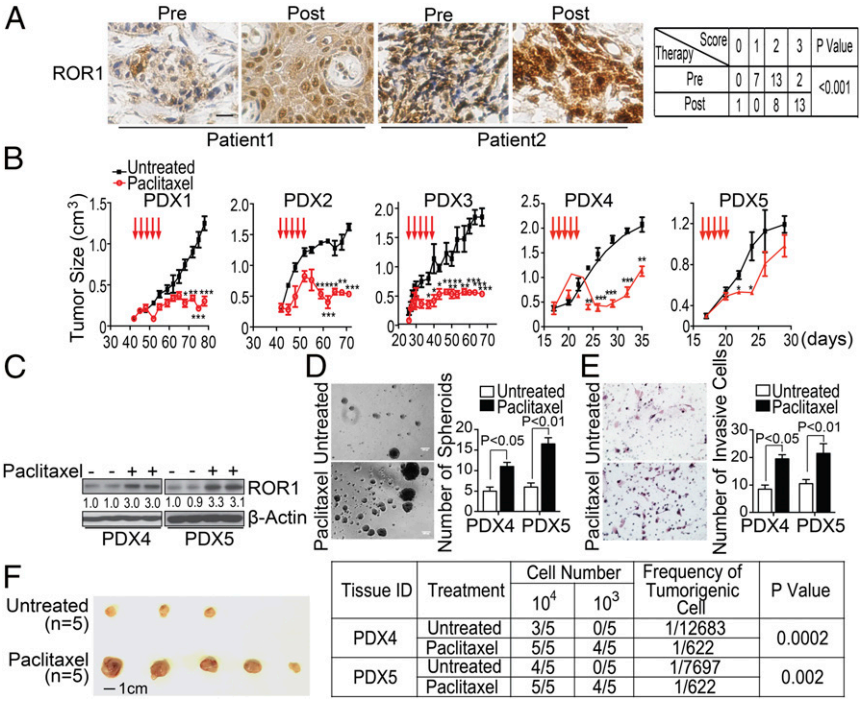

Tissue ID	Treatment	Cell Number 10^4	Cell Number 10^3	Frequency of Tumorigenic Cell	P Value
PDX4	Untreated	3/5	0/5	1/12683	0.0002
	Paclitaxel	5/5	4/5	1/622	
PDX5	Untreated	4/5	0/5	1/7697	0.002
	Paclitaxel	5/5	4/5	1/622	

Fig. 1. Chemotherapy enhances breast cancer expression of ROR1 and stemness. (*A*) Immunohistochemical staining of ROR1 in breast biopsy specimens obtained from patients ($n = 22$) before (Pre) or after (Post) therapy with docetaxel/epirubicin ± cyclophosphamide. (Scale bar: 25 μM.) The table to the *Right* shows the elevation of ROR1 on the breast cancer clinical specimens obtained from patients after chemotherapy treatment as assessed by Fisher's exact test. (*B*) The graph depicts the mean tumor growth of breast cancer PDXs in animals that did not receive treatment (black line, $n = 7$) or had received paclitaxel (red line, $n = 5$) on the days indicated by the red arrows. (*C*) Lysates from PDX4 or PDX5 isolated from untreated mice (–) or mice treated with paclitaxel (+) were examined for ROR1 or β-actin, which served to monitor the amount of protein per lane. The numbers below each lane are the ratios of band densities of ROR1 to β-actin normalized to that for the PDXs isolated from untreated mice. (*D* and *E*) The histograms depict the average numbers of spheroids (*D*) or invading cells (*E*) from PDX4 or PDX5 excised from mice that did not receive treatment (open bars, $n = 3$) or that were treated with paclitaxel (black bars, $n = 3$) ± standard error of the mean (SEM). Representative photomicrographs to the *Left* of the histograms depict the spheroids or invasive cells of PDXs excised from untreated mice or from mice that received paclitaxel. (Scale bar: 100 μm.) (*F*) Tumor cells were isolated from PDX4 or PDX5 mice that did not receive treatment (Untreated) or were treated with paclitaxel (Paclitaxel) as indicated on the *Left*. Isolated tumor cells from each PDX were reimplanted into mice ($n = 5$), and the tumor incidence was recorded. The *Left* provides representative photographs for tumors isolated from untreated mice or from mice that received paclitaxel. The frequency of tumorigenic cells and the probability estimates are shown on the *Right* using the extreme limiting dilution analysis (ELDA) software.

of both CD44 and CD24 ($CD44^+/CD24^+$ cells) (*SI Appendix*, Fig. S1 *B–D*).

In tissue cultures, the PDX cells that had expressed high levels of ROR1 had a greater capacity to form spheroids than PDX cells of the same tumor that had low-to-undetectable ROR1 (*SI Appendix*, Fig. S1 *E–G*). Furthermore, the tumor cells of each PDX that had high-level ROR1 were more invasive in Matrigel than tumor cells of the same PDX with low-to-undetectable ROR1 (*SI Appendix*, Fig. S1*H*).

We implanted equal numbers of tumor cells from each PDX into $Rag2^{-/-}\gamma_c^{-/-}$ mice and monitored the growth of secondary tumors. When these secondary tumors reached ~300 mm^3 in size, we treated the mice with paclitaxel at 13.4 mg/kg per day for five consecutive days (Fig. 1*B*). The tumors derived from the PDX with high proportions of $ROR1^+$ cells (e.g., PDX4 or PDX5) regrew shortly after therapy, in contrast to the tumors of mice engrafted with the PDX that had few $ROR1^+$ cells (e.g., PDX1 or PDX2, Fig. 1*B*).

We excised the tumors from mice bearing PDX4 or PDX5 and examined the human breast cancer cells for the expression of ROR1. We found the breast cancer PDXs excised from paclitaxel-treated mice expressed higher levels of ROR1 than the PDXs derived from the same tumor but excised from mice that did not receive paclitaxel or the original PDXs (Fig. 1*C*). As noted in prior studies (31), the tumors of mice treated with paclitaxel also had higher proportions of $ALDH1^+$ cells than the matched tumors of untreated mice or the original PDX (*SI Appendix*, Fig. S1*I*). Finally, the PDX cells excised from mice treated with paclitaxel had a greater capacity to form spheroids, invade Matrigel, or reengraft $Rag2^{-/-}\gamma_c^{-/-}$ mice than the PDXs derived from the same tumor but excised from mice that did not receive treatment or the original PDX (Fig. 1 *D–F*).

We isolated breast cancer cells that had high levels of ROR1 ($ROR1^{Hi}$) or low levels of ROR1 ($ROR1^{Low}$) from PDX3, PDX4, or PDX5 via flow cytometry using 4A5 (*SI Appendix*, Fig. S2*A*), a mAb that binds an epitope of ROR1 that is distinct from that bound by cirmtuzumab. $ROR1^{Hi}$ cells formed significantly greater numbers of spheroids than $ROR1^{Low}$ cells, which formed few spheroids or none at all (*SI Appendix*, Fig. S2*B*). Furthermore, $ROR1^{Hi}$ cells were significantly more invasive in Matrigel than $ROR1^{Low}$ cancer cells of the same tumor (*SI Appendix*, Fig. S2*C*).

We performed tumorigenicity assays with limiting numbers of tumor cells from PDX3, PDX4, or PDX5. Five hundred $ROR1^{Hi}$ cells from each PDX could establish secondary PDXs in most mice (*SI Appendix*, Fig. S2*D*). In contrast, the same numbers of $ROR1^{Low}$ cells did not form tumors except in a few animals (*SI Appendix*, Fig. S2*D*). Similarly, $ALDH1^+$ or $CD44^+/CD24^{Low}$ cells isolated from these PDXs also had a significantly greater capacity to form secondary PDXs than $ALDH1^{Neg}$ or $CD44^+/CD24^+$ cells of the same PDX (*SI Appendix*, Table S3), in agreement with prior studies (1, 7, 30).

Expression of ROR1 Associates with Activation of Hippo-YAP/TAZ and BMI1. We interrogated the PubMed Gene Expression Omnibus (GEO) database (accession no. GSE87455) on HER2-negative breast tumor biopsies obtained from patients before or after treatment with four cycles of epirubicin plus docetaxel and bevacizumab (2). Forty-three (76%) of the 57 post-treatment biopsy specimens had higher levels of *ROR1* than the matched pretreatment tumor specimens. Similarly, 48 (84%) of the matched tumor specimens had higher levels of *ALDH1A1* after therapy (*SI Appendix*, Fig. S3*A*). However, we did not observe a significant difference in the levels of *WNT5A* between pre- and post-treatment tumor samples (*SI Appendix*, Fig. S2*A*). Gene set enrichment (GSE) analysis revealed that post-treatment breast cancer cells had higher-level expression of genes associated with the activation of Rho-GTPases, Hippo-YAP/TAZ, or BMI1 than matched pretreatment tumor specimens (*SI Appendix*, Fig. S3*B*). Compared with matched pretreatment breast cancer-biopsy specimens, the breast cancer tissue obtained from patients after chemotherapy expressed higher levels of genes associated with EMT, $CD44^+/CD24^{Low}$ CSCs, or mammosphere- (MS-) forming cells (*SI Appendix*, Fig. S3*B*).

We segregated the pretreatment specimens (n = 122) of GSE87455 into two subgroups based upon their relative expression of *ROR1*. Samples with *ROR1* levels greater than the median level expressed in all samples were designated as $ROR1^{Hi}$ (n = 61), whereas tumor samples with lower *ROR1* were designated as $ROR1^{Low}$. The differences in gene expression between matched post- and pretreatment specimens resembled those of $ROR1^{Hi}$ versus $ROR1^{Low}$ breast cancers.

Of the 34,694 genes analyzed, we identified the 1,000 most overexpressed and the 1,000 most underexpressed genes differentially expressed in post-treatment versus pretreatment breast cancer specimens or in $ROR1^{Hi}$ versus $ROR1^{Low}$ breast cancers. Three-hundred-sixty-five of the 1,000 most overexpressed transcripts after chemotherapy were among the 1,000 most overexpressed in $ROR1^{Hi}$ cancers relative to $ROR1^{Low}$ breast cancers (e.g., *ALDH1A1*); only three of these 1,000 genes were among the 1,000 most overexpressed in $ROR1^{Low}$ tumors relative to $ROR1^{Hi}$ tumors ($P < 0.0001$, Fisher's exact test). Conversely, 190 of the 1,000 most underrepresented transcripts after chemotherapy were among the 1,000 most under-represented in $ROR1^{Hi}$ breast cancers relative to $ROR1^{Low}$ breast cancers; none of the 1,000 most under-represented genes after chemotherapy were under-represented in $ROR1^{Low}$ tumors relative to $ROR1^{Hi}$ cancers ($P < 0.0001$, Fisher's exact test). GSE analysis revealed that, relative to $ROR1^{Low}$ tumors, $ROR1^{Hi}$ tumors expressed higher levels of genes associated with the activation of Rho-GTPases (32, 33), Hippo-YAP/TAZ (34), BMI1 (35), or EMT (36) (*SI Appendix*, Fig. S3*C*). Similar findings were observed for samples described in the GSE21974 dataset (*SI Appendix*, Fig. S3 *D* and *E*).

Moreover, compared with $ROR1^{Low}$ tumors, $ROR1^{Hi}$ breast cancers also had higher expression of genes that were distinctively overexpressed in embryonic stem cells, including those activated by Oct4 or overlapping targets of Nanog, Oct4, and Sox2 (*SI Appendix*, Table S4) (37). Finally, $ROR1^{Hi}$ breast cancers expressed higher levels of genes that distinctively were overexpressed by $CD44^+/CD24^{Low}$ CSCs or MS-forming cells relative to $CD44^+/CD24^+$ non-CSCs or all tumor cells (1). Collectively, these analyses indicate that therapy induced changes in gene expression that more resembled those distinguishing $ROR1^{Hi}$ from $ROR1^{Low}$ breast cancers, potentially reflecting treatment-related increases in the proportions of $ROR1^+$ cells and/or increased expression of genes induced by ROR1 signaling rather than a direct effect of chemotherapy per se.

Wnt5a Induces ROR1-Dependent Activation of Rho-GTPases, YAP/TAZ, and BMI1. We extinguished *ROR1* via CRISPR/Cas9 in the basal-type breast cancer cell-line Hs578T (Fig. 2*A*). Exogenous Wnt5a could induce activation of Rac1, RhoA, and cdc42 within 10 min in wild-type Hs578T cells (wt-Hs578T) but not in $ROR1^{-/-}$ Hs578T cells lacking ROR1 ($ROR1^{-/-}$ Hs578T) (Fig. 2*A*). Treatment with Wnt5a also enhanced expression and nuclear localization of YAP/TAZ in wt-Hs578T cells but not in $ROR1^{-/-}$ Hs578T (Fig. 2 *B* and *C*).

Moreover, treatment with exogenous Wnt5a for 2 h enhanced expression of BMI1 protein but not *BMI1* messenger RNA in wt-Hs578T cells but not $ROR1^{-/-}$ Hs578T cells (Fig. 2*D* and *SI Appendix*, Fig. S4*A*), suggesting that Wnt5a induced increases in BMI1 by interfering with its degradation.

We examined whether Wnt5a could induce Hs578T cells to activate AKT, which prior studies found could inhibit proteasomal degradation and promote accumulation of BMI1 (38). Wnt5a induced AKT phosphorylation in wt-Hs578T cells but not in $ROR1^{-/-}$

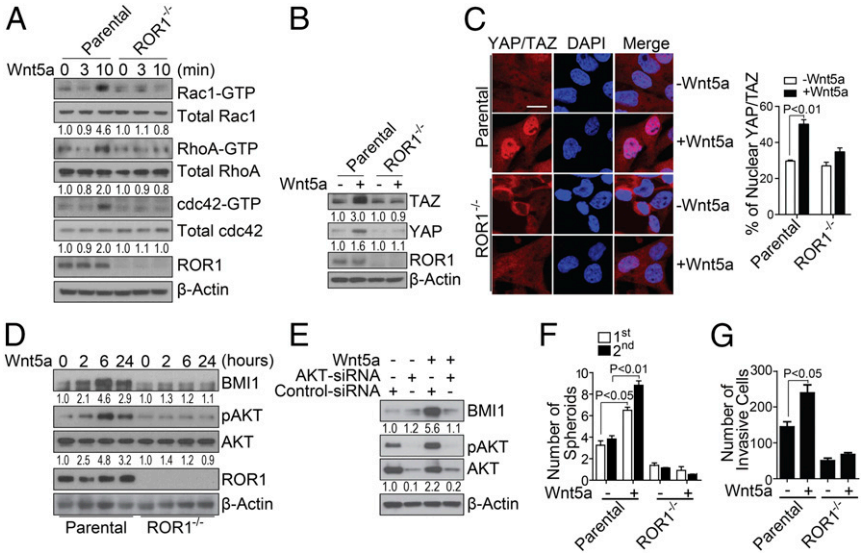

Fig. 2. Wnt5a induces ROR1-dependent activation of Rho-GTPases, YAP/TAZ, and BMI1. (*A*) Immunoblot analyses for proteins as indicated on the right using lysates prepared from Hs578T cells (Parental) or Hs578T knocked out for ROR1 (ROR1$^{-/-}$) that were stimulated with Wnt5a for the times indicated. The numbers below each lane are the ratios of the band densities of activated versus total GTPase, normalized with respect to cells treated without Wnt5a. (*B*) Immunoblot analyses for proteins indicated on the right using lysates from parental or ROR1$^{-/-}$ Hs578T that were treated without (–) or with (+) Wnt5a as indicated. The numbers below each lane represent the ratios of the band densities for each protein relative to that of β-actin, normalized with respect to cells treated without Wnt5a. (*C*) Photomicrographs of parental (*Top* row) or ROR1$^{-/-}$ Hs578T cells (*Bottom* row) that were treated without or with Wnt5a as indicated and then stained for YAP/TAZ and 4′,6-diamidino-2-phenylindole (DAPI) as indicated and then examined using confocal microscopy. (Scale bar: 20 μm.) The histogram to the *Right* of the photomicrographs provides the average percentages of YAP/TAZ located within the nuclei of the cells in each field (n = 10, ±SEM). (*D*) Immunoblot analyses for proteins indicated on the right using lysates of parental or ROR1$^{-/-}$ Hs578T (as indicated on the *Bottom*) that were treated with Wnt5a for the times indicated. The numbers below each lane are the ratios of band densities of BMI1 versus β-actin or pAKT versus total AKT normalized to that of the sample collected at time 0. (*E*) Immunoblot analyses for proteins indicated on the right using lysates of Hs578T that had been treated with control small interfering RNA (siRNA) or AKT-specific siRNA (AKT-siRNA) as indicated. The numbers below each lane are as in Fig. 3*D*. (*F* and *G*) The histograms depict the average numbers of spheroids (*F*) or invasive cells (*G*) from parental or ROR1$^{-/-}$ Hs578T that were treated without or with Wnt5a in triplicate ±SEM.

Hs578T cells (Fig. 2*D*). On the other hand, treatment of wt-Hs578T with siRNA specific for AKT or a small molecule inhibitor of AKT (MK-2206) impaired the capacity of Wnt5a to induce activation of AKT and inhibited the capacity of Wnt5a to enhance expression of BMI1 (Fig. 2*E* and *SI Appendix*, Fig. S4*B*). Functionally, ROR1$^{-/-}$ Hs578T cells formed significantly fewer spheroids than wt-Hs578T cells (Fig. 2*F*). Also, treatment with exogenous Wnt5a enhanced the capacity of wt-Hs578T cells but not ROR1$^{-/-}$ Hs578T to invade Matrigel (Fig. 2*G*).

Cirmtuzumab Inhibits Wnt5a-Induced Activation of Rho-GTPases, Hippo-YAP/TAZ, and BMI1 in Breast Cancer. We examined whether cirmtuzumab could inhibit Wnt5a-induced activation of Rho-GTPases, Hippo-YAP/TAZ, or BMI1. Treatment of wt-Hs578T cells with cirmtuzumab but not a human immunoglobulin G (hIgG) of irrelevant specificity, inhibited the capacity of exogenous Wnt5a to induce activation of Rac1, RhoA, or cdc42 (Fig. 3*A*), nuclear localization of TAZ (Fig. 3 *B* and *C*), activation of AKT, or expression of BMI1 (Fig. 3 *D* and *E*). Furthermore, treatment with cirmtuzumab but not control hIgG could block Wnt5a from enhancing the capacity of wt-Hs578T to form spheroids (Fig. 3*F*) or invade Matrigel (Fig. 3*G*). Similarly, we found that breast cancer PDX cells, which express Wnt5a (*SI Appendix*, Fig. S5*A*), had significantly less nuclear TAZ after treatment for 4 h with cirmtuzumab than the same breast cancer cells treated with control hIgG (*SI Appendix*, Fig. S5*B*). Moreover, cirmtuzumab but not control hIgG could reduce the expression of BMI1 in breast cancer PDX cells within 6 h (*SI Appendix*, Fig. S5*C*) and inhibit the capacity of these cells to form spheroids or invade Matrigel (*SI Appendix*, Fig. S5 *D* and *E*).

Cirmtuzumab Inhibits Reengraftment of Breast Cancer PDXs. We evaluated the activity of cirmtuzumab on breast cancer PDXs in vivo and found that biweekly intravenous infusions of cirmtuzumab (at 10 mg/kg) significantly suppressed the development and growth of PDX tumors, including PDX3, which had low-level expression of ROR1 (Fig. 4*A* and *SI Appendix*, Figs. S1*E* and S5 *F* and *G*). Moreover, treatment of mice bearing breast cancer PDXs with cirmtuzumab inhibited the development of pulmonary metastases, significantly reducing the numbers of metastatic foci from those noted in control hIgG-treated mice (Fig. 4*B*).

We examined the transcriptomes of breast cancer PDXs excised from cirmtuzumab-treated mice (n = 4) versus control-hIgG-treated mice (n = 4) and performed GSE analysis on the RNA-seq data (GSE108632). Tumor cells isolated from breast cancer PDXs of cirmtuzumab-treated mice expressed significantly lower levels of genes associated with the activation of Rho-GTPases, Hippo-YAP, BMI1, or EMT than cancer cells of the same PDXs isolated from control-hIgG-treated mice (Fig. 4*C* and *SI Appendix*, Fig. S5*H*). Moreover, tumors of cirmtuzumab-treated mice also expressed significantly lower levels of genes overexpressed by CD44^{+}/CD24^{Low} CSC or MS-forming cells (Fig. 4*C*) than did matched tumors of control-hIgG-treated mice. The PDXs of cirmtuzumab-treated mice also had lower levels of ROR1, activated Rho-GTPases, YAP/TAZ, or BMI1 than matched PDXs excised from control-treated mice as assessed by immunoblot analyses (Fig. 4*D*).

We examined PDX cells from control-treated or cirmtuzumab-treated mice for their capacity to form secondary PDXs in Rag2$^{-/-}\gamma_c^{-/-}$ mice. PDX cells isolated from cirmtuzumab-treated mice were significantly less effective in forming secondary PDXs

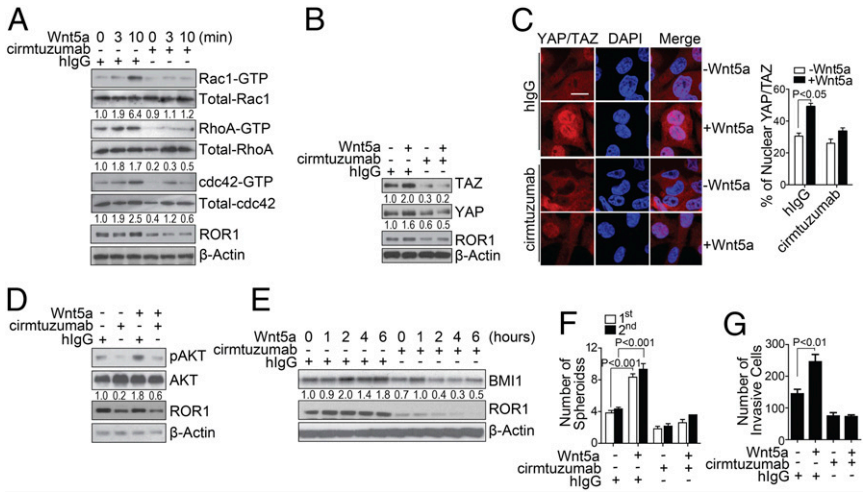

Fig. 3. Cirmtuzumab inhibits Wnt5a-induced ROR1-dependent activation of Rho-GTPases, YAP/TAZ, and BMI1. (*A*) Immunoblot analyses for proteins indicated on the right using lysates of Hs578T that had been treated with a control hIgG or cirmtuzumab and then stimulated with Wnt5a for the times indicated. The numbers below each lane are the ratios of the band densities of activated versus total GTPase, normalized with respect to the hIgG-treated cells without Wnt5a. (*B*) Immunoblot analyses for proteins indicated on the right using lysates prepared from Hs578T cultured with cirmtuzumab or hIgG and then treated without or with Wnt5a as indicated. The numbers below each lane represent the ratios of the band densities for each protein relative to that of β-actin, normalized with respect to the hIgG-treated cells without Wnt5a. (*C*) Photomicrographs of Hs578T cultured overnight with cirmtuzumab or hIgG (as indicted on the *Left*), then treated without or with Wnt5a for 4 h (as indicated), then stained for YAP/TAZ and DAPI (as indicated), and then examined via confocal microscopy. (Scale bar: 20 μm.) The histogram to the *Right* of the photomicrographs provides the average percentages of YAP/TAZ located within the nuclei of the cells in each field ($n = 10$, ±SEM). (*D*) Immunoblot analyses for proteins indicated on the right using lysates of Hs578T that had been treated overnight with hIgG or cirmtuzumab and then treated without or with Wnt5a as indicated. The numbers below each lane are the ratios of band densities of pAKT versus total AKT, normalized with respect to the hIgG-treated cells without Wnt5a. (*E*) Immunoblot analyses for proteins indicated on the right using lysates of Hs578T that had been treated overnight with hIgG or cirmtuzumab and then treated with Wnt5a for the times indicated. The numbers below each lane are the ratios of band densities of BMI1 versus β-actin, normalized with respect to the hIgG-treated cells without Wnt5a. (*F* and *G*) The bar graph depicts the average numbers of spheroids (*F*) or invasive cells (*G*) from Hs578T cells that were incubated with hIgG or cirmtuzumab overnight and then treated with or without Wnt5a in three separate culture wells ± SEM. The open bars indicate the number of spheroids detected during the first passage, whereas the closed bars provide those of the second passage in three separate culture wells ± SEM.

than tumor cells of the same PDXs isolated from mice treated with hIgG (Fig. 4*E*). Collectively, these data indicate that treatment with cirmtuzumab inhibited the stemness of breast cancer cells in vivo.

Treatment with Paclitaxel and Cirmtuzumab Achieves Greater Tumor Clearance than Treatment with Either Alone. We treated PDX4- or PDX5-bearing mice with cirmtuzumab (10 mg/kg), paclitaxel (13.4 mg/kg) (39), or the combination of cirmtuzumab and paclitaxel. Treatment with cirmtuzumab and paclitaxel was significantly more effective in reducing tumor volumes than treatment with either cirmtuzumab or paclitaxel alone (Fig. 5*A*), each of which significantly inhibited tumor growth relative to that of control-treated animals. The tumor cells isolated from the PDXs of mice treated with cirmtuzumab and paclitaxel had lower levels of ROR1, activated Rho-GTPases, phosphorylated AKT, YAP/TAZ, and BMI1 than did the tumor cells of the same PDXs excised from mice treated with paclitaxel alone (Fig. 5*B*). These data demonstrate that the combination of cirmtuzumab and paclitaxel had complementary antitumor activity.

We isolated tumor cells of PDXs that recurred in animals after therapy and studied their relative capacity to form secondary PDXs when engrafted in other immune-deficient mice. We found that the tumor cells of the PDXs from mice treated with single-agent paclitaxel readily developed secondary PDXs. However, the tumor cells isolated from cirmtuzumab-treated mice were significantly less effective in generating secondary PDXs than the tumor cells isolated from animals treated with paclitaxel or hIgG. However, none of the mice engrafted with tumor cells isolated from mice treated with cirmtuzumab and paclitaxel developed detectable tumors (Fig. 5*C*).

Discussion

Tumor recurrence following treatment with chemotherapy may develop from chemotherapy-resistant preexisting CSCs or from enduring cancer cells that subsequently acquire self-renewing and/or tumor-initiating capacities, resulting from chemotherapy-induced changes in the tumor or its microenvironment (niche signaling) (40, 41). Here, we report that breast cancer cells surviving chemotherapy expressed higher levels of ROR1, which was associated with the activation of pathways induced by ROR1 signaling (e.g., Hippo-YAP/TAZ and BMI1). Blocking ROR1 signaling with the humanized anti-ROR1 mAb cirmtuzumab diminished the activation of such pathways, the development of metastases, or the capacity of cancer cells to persist after chemotherapy.

ROR1 signaling may contribute to the maintenance, self-renewal, and drug resistance of cancer cells. Consistent with this notion, we found that expression of genes associated with the activation of Rho-GTPases was increased in breast cancer cells with high levels of ROR1. Prior studies found that Rho-GTPase signaling is altered in human breast tumors, and the elevated expression and activation of Rho-GTPases correlates with tumor progression, metastasis, and poor prognosis (23, 42). Furthermore, the activation of Rac1 may promote the survival of breast cancer cells during radiation therapy (24).

High-level expression of ROR1 in primary breast cancer also was associated with high levels of BMI1. Wnt5a/ROR1 signaling may enhance the expression of BMI1 through its capacity to activate AKT, which can phosphorylate BMI1 at three highly conserved serine residues thereby reducing the rate of BMI1 protein degradation (43). The resulting increase in BMI1 may account, in part, for the enhanced capacity of $ROR1^{Hi}$ breast cancer cells to initiate tumor growth, spread to distal sites, or resist the cytotoxic effects of chemotherapy relative to breast cancer cells lacking

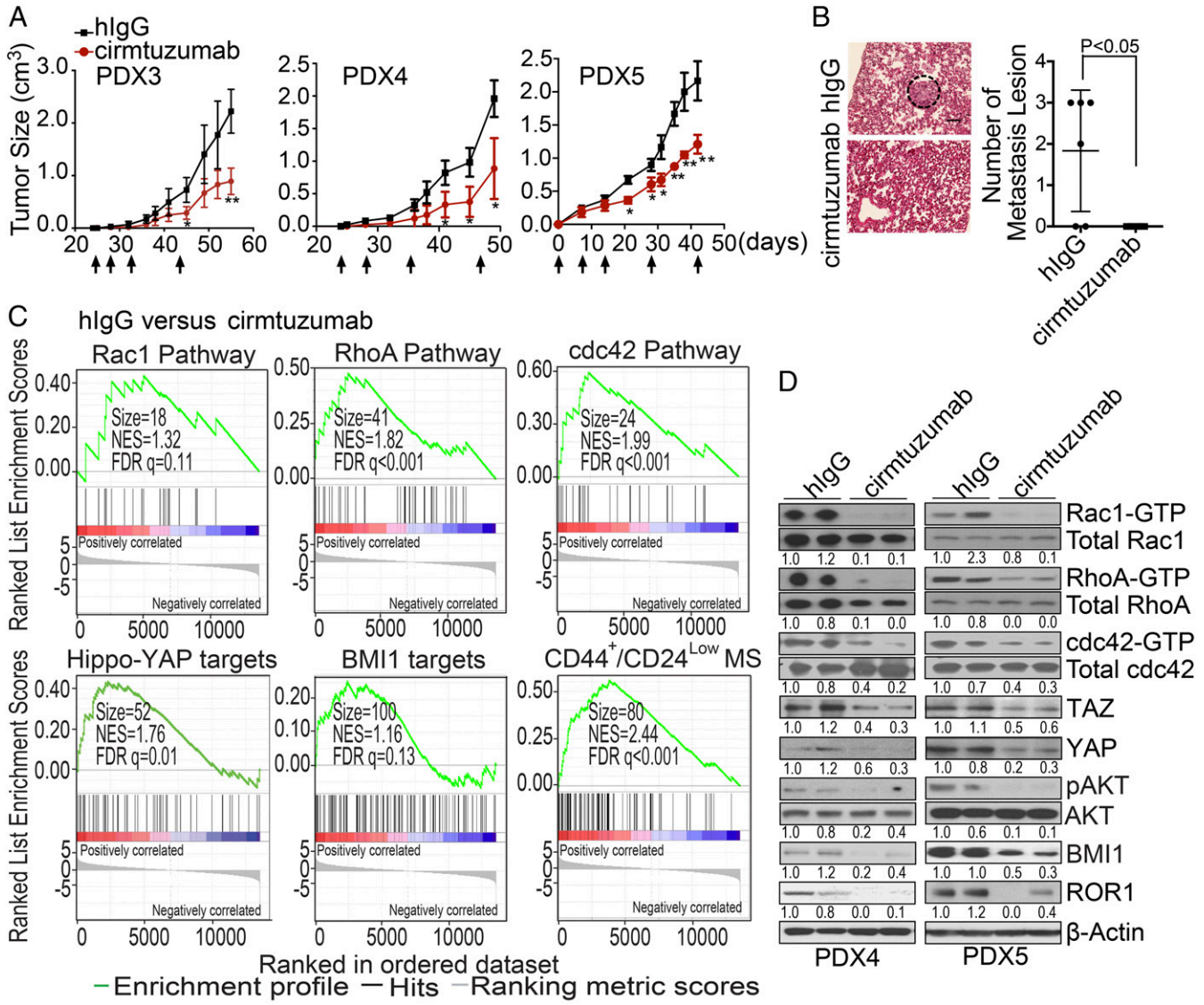

E

	Treatment	Cell Number			Frequency of Tumorigenic Cell	P Value
		1X10^5	1X10^4	1X10^3		
PDX3	hIgG	8/9	5/12	N.D	1/31648	0.03
	cirmtuzumab	2/4	1/8	N.D	1/120416	
PDX4	hIgG	10/10	10/10	0/5	1/3285	8.61e-13
	cirmtuzumab	2/10	1/10	0/5	1/247052	
PDX5	hIgG	N.D	5/5	2/4	1/1420	0.001
	cirmtuzumab	N.D	1/5	1/3	1/23572	

Fig. 4. Cirmtuzumab inhibits stemness of breast cancer PDXs. (*A*) The line graph depicts the mean tumor growth of each of PDX3, PDX4, and PDX5 over time (±SEM, $n = 6$–8) for animals that did not receive treatment (black line) or that were treated with cirmtuzumab (red line) on the days indicated by the black arrows. One asterisk indicates $P < 0.05$, and two asterisks indicate $P < 0.01$ using Student's *t Test*. (*B*) Hematoxylin and eosin staining of lung tissue from a representative tumor-bearing mouse engrafted with cells of PDX5 and treated with control hIgG or cirmtuzumab as indicated. A dashed-lined circle highlights metastatic foci. (Scale bar: 100 μm.) The scatter plot shows the average numbers of metastatic foci that were found in the lungs of each animal by the treatment group (±SEM, $n = 6$). (*C*) Enrichment plots of genes associated with the activation of Rho-GTPases, Hippo-YAP, BMI1, or gene signature common on both CD44$^+$/CD24^{Low} cancer stem cells and MS-forming cells in PDXs derived from PDX4 in mice treated with control hIgG versus cirmtuzumab as assessed via RNA sequencing (RNA-seq) (GSE108632). (*D*) Immunoblot analyses for proteins indicated on the right using lysates prepared from PDX4 or PDX5 (as indicated on the *Bottom*) that were extirpated from mice treated with control hIgG or cirmtuzumab as indicated. The numbers below each row are the ratios of band densities of activated versus total GTPase, pAKT versus total AKT, BMI1, TAZ/YAP versus β-actin, or ROR1 versus β-actin, normalized to that of the first control sample. (*E*) Table providing the numbers of mice that developed tumors (numerator) versus the numbers of mice implanted (denominator) with cells from PDX3, PDX4, or PDX5 (as indicated in the left column), which were removed from mice treated with either hIgG or cirmtuzumab (as indicated in the second column). For these experiments, mice were given varying numbers of tumor cells (as indicated in the row below "cell number"). The frequencies of tumorigenic cells computed using ELDA software are provided in the penultimate right column. The *P* values indicate the significance of the difference between the tumorigenic frequencies of tumor cells recovered from hIgG- versus cirmtuzumab-treated mice.

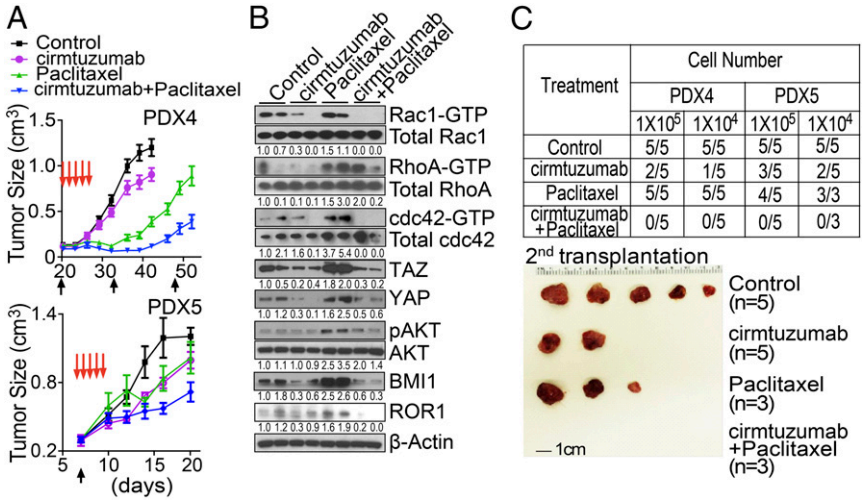

Treatment	Cell Number			
	PDX4		PDX5	
	$1X10^5$	$1X10^4$	$1X10^5$	$1X10^4$
Control	5/5	5/5	5/5	5/5
cirmtuzumab	2/5	1/5	3/5	2/5
Paclitaxel	5/5	5/5	4/5	3/3
cirmtuzumab +Paclitaxel	0/5	0/5	0/5	0/3

Fig. 5. Cirmtuzumab and paclitaxel have complementary antitumor activity. (*A*) The line graph depicts the mean tumor growth of PDX4 or PDX5 over time (±SEM, $n = 8–10$) in mice that were untreated (Control, black line) or treated with cirmtuzumab (purple line), paclitaxel (green line), or both (blue line). (*B*) Immunoblot analyses for proteins indicated on the right using lysates prepared from PDX4 of mice that were not treated (Control) or treated with cirmtuzumab, paclitaxel, or both as indicated. The numbers below each row are the ratios of band densities as in Fig. 4*E*. (*C*) Table providing the numbers of mice that developed PDXs (numerator) versus the numbers of mice engrafted (denominator) with cells from either PDX4 or PDX5 (as indicated in the top row) that were removed from mice treated with hIgG, cirmtuzumab, paclitaxel, or cirmtuzumab and paclitaxel (as indicated in the far left column). The mice were given varying numbers of tumor cells as indicated in the row below the PDX designation. The *Bottom* provides a photograph of representative tumors that developed in mice engrafted with tumor cells from PDX4 of mice that were untreated or treated with cirmtuzumab and/or paclitaxel as indicated.

ROR1. Conversely, inhibiting BMI1 with a small molecule PTC-209 could enhance the sensitivity to chemotherapy and inhibit metastases in squamous cell carcinoma or inhibit the growth of colon cancer or breast cancer cells (12, 44).

The stemness of $ROR1^{Hi}$ breast cancer cells, in part, also could be related to the activation of the Hippo-YAP/TAZ pathway. Prior studies found that Rho-GTPase activation could induce the Hippo-YAP/TAZ signaling, which could enhance the survival and self-renewal of human-embryonic stem cells (25). Moreover, coexpression of ROR1 with either FZD2 or FZD5 could induce dephosphorylation YAP and the accumulation of TAZ, leading to the activation of Hippo-YAP/TAZ signaling in HEK293A cells (26). Similarly, we found the expression of ROR1 was associated with the expression and nuclear localization of TAZ in primary breast cancer cells and that Wnt5a could enhance nuclear accumulation of TAZ in a ROR1-dependent manner. Furthermore, the expression of ROR1 also could promote EMT, which could enable epithelial breast cancer cells to migrate to distal sites (17).

The anti-ROR1 mAb cirmtuzumab may be effective in reversing cancer stemness. In a recently completed phase I trial involving patients with relapse/refractory CLL, treatment with cirmtuzumab inhibited leukemia-cell activation of Rho-GTPases and ROR1-signaling (14). Moreover, treatment with cirmtuzumab reversed the stemness gene expression signature of leukemia cells noted before therapy (14). This is similar to what we noted here in studies using mice engrafted with breast cancer PDXs; treatment with cirmtuzumab but not control hIgG repressed the expression of genes induced by the activation of Rho-GTPases, Hippo-YAP/TAZ, or BMI1. Moreover, cirmtuzumab also repressed the expression of genes that were upregulated in EMT or $CD44^+/CD24^{Low}$ CSC. Such reprogramming was associated with impaired engraftment and reduced capacity to develop metastases in immune-deficient mice.

Agents that inhibit cancer stemness may complement the antitumor activity of chemotherapy by eliminating drug-resistant CSC or inhibiting the capacity of tumor cells to acquire features of CSCs. We found that treatment of either ER^+ or ER^- breast cancer PDXs with paclitaxel and cirmtuzumab had significantly greater antitumor activity than treatment with either agent alone. We speculate that cirmtuzumab or other agents that can inhibit ROR1 signaling may improve the response to chemotherapy and enhance the survival of patients with breast cancer.

Materials and Methods

Breast Cancer Specimens. We used anonymized archived formalin-fixed paraffin-embedded tumor tissues excised from patients ($n = 22$) with invasive ductal carcinoma before and after treatment with four to six cycles of docetaxel (T) at 75 mg/m^2 ± doxorubicin (A) at 75 mg/m^2 or epirubicin (E) at 75 mg/m^2 ± cyclophosphamide (C) at 600 mg/m^2 (docetaxel/epirubicin/doxorubicin, docetaxel/doxorubicin/cyclophosphamide, docetaxel/epirubicin, or epirubicin and cyclophosphamide) at Sun Yat-set University Cancer Center, China. Each patient had a core needle biopsy or excisional biopsy before neoadjuvant chemotherapy and had surgical resection of residual tumors after chemotherapy.

Primary breast tumor tissues used to generate PDXs were obtained from biopsy material of patients with breast adenocarcinoma after they provided written informed consent. Experiments involving these samples were approved by the Institutional Review Board of UC San Diego (HRPP090401) in accordance with the Declaration of Helsinki.

Spheroid Formation Assay. Some 300–10,000 viable single cells were plated on Ultra Low Attachment 6-well or 96-well plates (Corning Incorporated Life Sciences) and cultured in MEGMTM mammary epithelial cell growth medium (Lonza) with or without recombinant Wnt5a (R&D system) at 100 ng/mL for 1–3 wk. Spheroids with sizes greater than 100 μm were counted using an inverted microscope (Nikon). A more detailed description of the reagents, biochemistry assays, cellular analysis, and animal studies are provided in *SI Appendix, Materials and Methods*.

ACKNOWLEDGMENTS. We thank Victoria Tripple for technical assistance in the PDX studies and Dennis Young for flow-cytometry analysis and sorting. We acknowledge the help of the Histology Core Laboratory for processing tissue specimens, Dr. Nissi Varki for histology and immunohistochemistry assessments, and the University of California San Diego Moores Cancer Center Biorepository and Tissue Technology Shared Resource for PDX samples. This paper was supported by the National Key Projects of Research and Development of China (Grant 2016YFC0904600), the National Natural Science Foundation of China (Grant 81672912), the Science and Technology Foundation of Shenzhen, China (Shenzhen Peacock Innovation Team Project, Grant KQTD20140630100658078), the Breast Cancer Research Foundation (Grant BCRF-17-120), National Institutes of Health Grant P01-CA081534, and the California Institute for Regenerative Medicine.

1. Creighton CJ, et al. (2009) Residual breast cancers after conventional therapy display mesenchymal as well as tumor-initiating features. *Proc Natl Acad Sci USA* 106: 13820–13825.
2. Kimbung S, et al.; PROMIX Trialists Group (2018) Assessment of early response biomarkers in relation to long-term survival in patients with HER2-negative breast cancer receiving neoadjuvant chemotherapy plus bevacizumab: Results from the Phase II PROMIX trial. *Int J Cancer* 142:618–628.
3. Ye X, et al. (2015) Distinct EMT programs control normal mammary stem cells and tumour-initiating cells. *Nature* 525:256–260.
4. Wahl GM, Spike BT (2017) Cell state plasticity, stem cells, EMT, and the generation of intra-tumoral heterogeneity. *NPJ Breast Cancer* 3:14.
5. Batlle E, Clevers H (2017) Cancer stem cells revisited. *Nat Med* 23:1124–1134.
6. Arteaga CL (2013) Progress in breast cancer: Overview. *Clin Cancer Res* 19:6353–6359.
7. Al-Hajj M, Wicha MS, Benito-Hernandez A, Morrison SJ, Clarke MF (2003) Prospective identification of tumorigenic breast cancer cells. *Proc Natl Acad Sci USA* 100: 3983–3988.
8. Wang Y, et al. (2012) Cancer stem cell marker Bmi-1 expression is associated with basal-like phenotype and poor survival in breast cancer. *World J Surg* 36:1189–1194.
9. Grinstein E, Mahotka C (2009) Stem cell divisions controlled by the proto-oncogene BMI-1. *J Stem Cells* 4:141–146.
10. Lukacs RU, Memarzadeh S, Wu H, Witte ON (2010) Bmi-1 is a crucial regulator of prostate stem cell self-renewal and malignant transformation. *Cell Stem Cell* 7: 682–693.
11. Wu X, et al. (2011) Silencing of Bmi-1 gene by RNA interference enhances sensitivity to doxorubicin in breast cancer cells. *Indian J Exp Biol* 49:105–112.
12. Kreso A, et al. (2014) Self-renewal as a therapeutic target in human colorectal cancer. *Nat Med* 20:29–36.
13. Paranjape AN, et al. (2014) Bmi1 regulates self-renewal and epithelial to mesenchymal transition in breast cancer cells through Nanog. *BMC Cancer* 14:785.
14. Choi MY, et al. (2018) Phase I trial: Cirmtuzumab inhibits ROR1 signaling and stemness signatures in patients with chronic lymphocytic leukemia. *Cell Stem Cell* 22:951–959.e3.
15. Zhang S, et al. (2012) ROR1 is expressed in human breast cancer and associated with enhanced tumor-cell growth. *PLoS One* 7:e31127.
16. Zhang S, et al. (2012) The onco-embryonic antigen ROR1 is expressed by a variety of human cancers. *Am J Pathol* 181:1903–1910.
17. Cui B, et al. (2013) Targeting ROR1 inhibits epithelial-mesenchymal transition and metastasis. *Cancer Res* 73:3649–3660.
18. Chien HP, et al. (2016) Expression of ROR1 has prognostic significance in triple negative breast cancer. *Virchows Arch* 468:589–595.
19. Fukuda T, et al. (2008) Antisera induced by infusions of autologous Ad-CD154-leukemia B cells identify ROR1 as an oncofetal antigen and receptor for Wnt5a. *Proc Natl Acad Sci USA* 105:3047–3052.
20. Pukrop T, et al. (2006) Wnt 5a signaling is critical for macrophage-induced invasion of breast cancer cell lines. *Proc Natl Acad Sci USA* 103:5454–5459.
21. Iozzo RV, Eichstetter I, Danielson KG (1995) Aberrant expression of the growth factor Wnt-5A in human malignancy. *Cancer Res* 55:3495–3499.
22. Yu J, et al. (2016) Wnt5a induces ROR1/ROR2 heterooligomerization to enhance leukemia chemotaxis and proliferation. *J Clin Invest* 126:585–598.
23. Fritz G, Just I, Kaina B (1999) Rho GTPases are over-expressed in human tumors. *Int J Cancer* 81:682–687.
24. Hein AL, et al. (2016) RAC1 GTPase promotes the survival of breast cancer cells in response to hyper-fractionated radiation treatment. *Oncogene* 35:6319–6329.
25. Ohgushi M, Minaguchi M, Sasai Y (2015) Rho-signaling-directed YAP/TAZ activity underlies the long-term survival and expansion of human embryonic stem cells. *Cell Stem Cell* 17:448–461.
26. Park HW, et al. (2015) Alternative Wnt signaling activates YAP/TAZ. *Cell* 162:780–794.
27. Cordenonsi M, et al. (2011) The Hippo transducer TAZ confers cancer stem cell-related traits on breast cancer cells. *Cell* 147:759–772.
28. Bartucci M, et al. (2015) TAZ is required for metastatic activity and chemoresistance of breast cancer stem cells. *Oncogene* 34:681–690.
29. Moroishi T, Hansen CG, Guan KL (2015) The emerging roles of YAP and TAZ in cancer. *Nat Rev Cancer* 15:73–79.
30. Ginestier C, et al. (2007) ALDH1 is a marker of normal and malignant human mammary stem cells and a predictor of poor clinical outcome. *Cell Stem Cell* 1:555–567.
31. Samanta D, Gilkes DM, Chaturvedi P, Xiang L, Semenza GL (2014) Hypoxia-inducible factors are required for chemotherapy resistance of breast cancer stem cells. *Proc Natl Acad Sci USA* 111:E5429–E5438.
32. Schaefer CF, et al. (2009) PID: The pathway interaction database. *Nucleic Acids Res* 37: D674–D679.
33. Liberzon A, et al. (2011) Molecular signatures database (MSigDB) 3.0. *Bioinformatics* 27:1739–1740.
34. Li C, et al. (2017) A ROR1-HER3-lncRNA signalling axis modulates the Hippo-YAP pathway to regulate bone metastasis. *Nat Cell Biol* 19:106–119.
35. Wiederschain D, et al. (2007) Contribution of polycomb homologues Bmi-1 and Mel-18 to medulloblastoma pathogenesis. *Mol Cell Biol* 27:4968–4979.
36. Taube JH, et al. (2010) Core epithelial-to-mesenchymal transition interactome gene-expression signature is associated with claudin-low and metaplastic breast cancer subtypes. *Proc Natl Acad Sci USA* 107:15449–15454.
37. Ben-Porath I, et al. (2008) An embryonic stem cell-like gene expression signature in poorly differentiated aggressive human tumors. *Nat Genet* 40:499–507.
38. Kim J, Hwangbo J, Wong PK (2011) p38 MAPK-mediated Bmi-1 down-regulation and defective proliferation in ATM-deficient neural stem cells can be restored by Akt activation. *PLoS One* 6:e16615.
39. Desai N, et al. (2006) Increased antitumor activity, intratumor paclitaxel concentrations, and endothelial cell transport of cremophor-free, albumin-bound paclitaxel, ABI-007, compared with cremophor-based paclitaxel. *Clin Cancer Res* 12:1317–1324.
40. Gilbert LA, Hemann MT (2010) DNA damage-mediated induction of a chemoresistant niche. *Cell* 143:355–366.
41. Milanovic M, et al. (2018) Senescence-associated reprogramming promotes cancer stemness. *Nature* 553:96–100.
42. McHenry PR, Vargo-Gogola T (2010) Pleiotropic functions of Rho GTPase signaling: A Trojan horse or Achilles' heel for breast cancer treatment? *Curr Drug Targets* 11: 1043–1058.
43. Nacerddine K, et al. (2012) Akt-mediated phosphorylation of Bmi1 modulates its oncogenic potential, E3 ligase activity, and DNA damage repair activity in mouse prostate cancer. *J Clin Invest* 122:1920–1932.
44. Srinivasan M, et al. (2017) Downregulation of Bmi1 in breast cancer stem cells suppresses tumor growth and proliferation. *Oncotarget* 8:38731–38742.

Supplementary Information

Materials and Methods

Patient-Derived Xenografts (PDX) and breast-cancer cell-lines

Four-to-eight-week-old female Rag2$^{-/-}\gamma_c^{-/-}$ mice were used to generate breast cancer PDX following guidelines for treatment of laboratory animals of United States National Institutes of Health (NIH). The UC San Diego Medical Experimental Animal Care Committee approved the study protocol. The mice were housed in laminar-flow cabinets under specific pathogen-free conditions and fed *ad libitum*. We enzymatically/mechanically dissociated breast cancer biopsy material into single cells and implanted washed, viable cells into Rag2$^{-/-}\gamma_c^{-/-}$ mice. Early passage (P1-P5) of primary tumor tissues from these PDX models were dissociated enzymatically/mechanically using *GentleMACS Dissociator* (Miltenyi Biotec), as per the manufacturer's guidelines. Erythrocytes were removed via density gradient centrifugation in Percoll Plus (GE Healthcare Life Sciences, CC-17-5442-01).

Hs578T cells were obtained from the American Type Culture Collection (ATCC, Manassas, VA) in 2017. The identity of each cell line was confirmed by short tandem repeat profiling of 10 loci using the GenePrint 10 system (Promega). *Mycoplasma* testing of cell cultures was carried out routinely using the MycoAlert Mycoplasma Detection Kit (Lonza), most recently in May 2018. Cells were passaged no more than 18 times before a low-passage batch was thawed. Cells were growing in DMEM containing 10% FBS and 10 µg/mL insulin.

Tumorigenicity assay

Cells were suspended in Mammary-Epithelial Growth Medium (MEGM), mixed with Matrigel (BD Biosciences, San Diego, CA) at a 1:1 ratio, and then transplanted into the mammary pads of $Rag2^{-/-}\gamma_c^{-/-}$ mice. We monitored the mice weekly for the development of tumors. We extirpated tumors to examine the breast cancer cells for expression of ROR1 at 10 days after treatment with 13.4 mg/kg paclitaxel delivered via intravenous injection on each of consecutive 5 days.

To examine for metastases, we harvested the lungs of 6 mice from each treatment group at 42- or 48-days after engraftment and fixed the tissue with 10%-formalin, prior to paraffin embedding. Each paraffin block was cut into 200-μm sections. Tumor foci were scored in a blinded fashion by a board-certified pathologist.

To test whether cirmtuzumab alone or in combination with paclitaxel affected the growth of primary breast tumor cells, $1x10^5$ single cells isolated from PDX4 or PDX5 were injected into the mammary pads of 4- to 6-week-old $Rag2^{-/-}\gamma_c^{-/-}$ mice. When the mice developed tumors of 300 mm^3 in size, they received paclitaxel at 13.4 mg/kg intravenously on each of 5 consecutive days and/or cirmtuzumab at 10 mg/kg intravenously twice, spaced 1 week apart, and then biweekly thereafter. Control groups were similarly treated instead with hIgG or irrelevant specificity. The tumor volume (v) was determined using the formula $v = (\text{length}) \times (\text{width})^2 \times 0.4$. Mice were monitored for 6- or 8-weeks after the implantation of tumor cells for tumor engraftment using an extreme limiting dilution assay.

RNA-Seq sample preparation and sequencing

Total RNA was prepared from tumor tissues excised using the Trizol RNA-extraction protocol with subsequent purification of RNA using RNeasy columns (Qiagen kit). Total RNA was assessed for quality using an Agilent Tapestation. Samples had RNA Integrity Numbers (RIN) ranging from 9.2 to 9.9. RNA libraries were generated from 1 μg of RNA using Illumina's TruSeq Stranded mRNA Sample Prep Kit, following the manufacturer's instructions, modifying the shear time to 5 minutes. RNA libraries were multiplexed and sequenced with 50 base pair (bp) single end reads (SR50) to a depth of approximately 40 million reads per sample on an Illumina HiSeq4000.

We applied standard RNA-seq analytical pipeline to the eight samples. Briefly, adapters were removed and reads were trimmed of bases with low quality scores in late sequencing cycles using Cutadapt, which removes adapter sequences from high-throughput sequencing reads (1). We then mapped the reads to human genome build 38, using the STAR aligner (v2.5.2b) (2). RSEM (v1.3.0) (3) was used to obtain the raw gene counts from the read alignments and Ensemble gene models (v83) (4). We used package DEseq2 (5) to normalize the read count data and Illumina software package to assess for differential expression. The data were deposited in a GEO database (GSE108632).

Gene set enrichment analyses

We used the GSEA software (6) for gene-set-enrichment analyses (GSEA) on the primary microarray data available in the GEO database under accession numbers GSE87455 (7) and GSE21974 (8). We also performed GSEA on RNA-Seq data (GSE108632) generated from PDX isolated mice treated with cirmtuzumab or control human IgG (hIgG). Microarray data, obtained from 50 breast cancer samples collected before (n=25) and

after (n=25) chemotherapy (Tx) (GSE21974) or from 122 breast cancer samples from GSE87455 dataset, were ranked by their relative expression of ROR1. Of these cases, tumors with a ROR1 expression value above the median for all samples were designated as $ROR1^{Hi}$, whereas tumors with ROR1 expression value below the median value were designated as $ROR1^{Low}$. We ranked genes by their association with the breast cancer groups ($ROR1^{Hi}$ versus $ROR1^{Low}$) using a GSEA signal-to-noise ratio ranking metric. We focused GSEA on 3 pathways: Rac1 in BIOCARTA database, cdc42 in Pathway Interaction Database (9, 10), and RhoA in Ingenuity Pathway database (IPA ®,QIAGEN Redwood City, www.qiagen.com/ingenuity). Each gene set was considered significant when the false discovery rate (FDR) was less than 25% (6). For each gene set tested, we determined the gene-set size (SIZE), the enrichment score (ES), the normalized ES (NES), the nominal p value (NOM p-val), and the FDR q value (FDR q-val). The FDR q value was adjusted for gene set size and multiple hypothesis testing.

Flow cytometry analysis

Single-cell suspensions were treated with Fc-blocking (Miltenyi Biotec), and then stained with Fluorescein-conjugated anti-CD44 (#555479), phycoerythrin (PE)-conjugated anti-CD24 (#561646, Pharmingen), Alexa-647-conjugated 4A5 (11), PE-conjugated anti-EpCAM (#347198, BD Biosciences), and phycoerythrin (PE)-conjugated anti-HLA-A2 (#343306, Biolegend). ALDH1 activity was detected according to method described previously (12). Data were acquired using a FACS-Calibur or FACS-Aria (Becton Dickinson) and were analyzed using the FlowJo software (Tree Star). Forward light scatter (FSC) and side-light scatter (SSC) gating was used to exclude cell debris. Furthermore, we excluded cells that stained with propidium iodide (PI, Sigma) and gated

on cells that stained with Calcein Violet (Life Technology) for viable cell analysis. Finally, gating on cells that bound to a mAb specific for human EpCAM allowed us to examine for breast cancer epithelial cells.

Cell-Invasion assay

$5x10^4$ viable single cells from primary tumors were suspended in MEBM growth medium (Lonza, MD), plated in invasion chambers (8-μm pore size, BD Biosciences), and cultured with or without cirmtuzumab (50 μg/ml) overnight. The lower chambers were filled with serum-free, conditioned medium collected from NIH3T3 cells. Invasion assay for cell lines were performed as described (13). The cells on the apical side of each insert were scrapped off. Invasive cells were fixed with 4% paraformaldehyde and stained by Diff-Quick staining kits (IMEB Inc, San Marcos, CA) and visualized with an inverted microscope (Nikon). A more detailed description of the reagents, biochemistry assays, cellular analysis and animal studies are provided in SI Appendix, Materials and Methods.

Immunohistochemistry staining

For immunohistochemistry staining, primary tumors or lung organs excised from mouse xenografts were fixed in formalin. Lung tissue sections were prepared and stained with Hematoxylin & Eosin (H&E), Hematoxylin, or anti-ROR1 antibody (4A5) as described previously (14). Images were collected using a Delta Vision microscope. The levels of ROR1 were scored on the following scale as described (14); A score of 0 indicated that none of the cancer cells in the sample stained with the anti-ROR1 mAb; a score of 1 indicated low-level binding of the mAb to the tumor cells or low-to-moderate-level binding of the mAb to less than 50% of tumor cells; a score of 2 indicates moderate-level staining on more than 50% of tumor cells or high-level staining of the tumor cells on less than 50%

of tumor cells; a score of 3 indicates high-level staining of the tumor cells on more than 50% of tumor cells. All staining was evaluated by a board-certificated pathologist.

Immunofluorescence staining

Cells were cultured on coverslips to appropriate density or spun onto slides using a cytocentrifuge. Cells were fixed with 4% paraformaldehyde and permeabilized with 0.1% Triton X-100 in PBS. After the cells were washed twice with PBS, they were blocked with 1% BSA in PBS for 30 minutes. Control antibodies or rabbit anti-YAP/TAZ (#8418, Cell Signaling Technology) or mouse 4A5 was added in blocking buffer and incubated for 1.5 hours. After washing the cells with PBS, they were incubated with Alexa Fluor 594-conjugated anti-rabbit secondary antibodies or Alexa Fluor 488-conjugated anti-mouse secondary antibodies for 1.5 hours. The cells were washed again and mounted onto slides using ProLong Gold Antifade Reagent with DAPI (Life Technologies). The images were obtained and analyzed by using an Olympus FV1000 confocal microscope. The percentage of the nuclear localized YAP/TAZ was analyzed by Intensity measurement of Image J software. Nuclear localized YAP/TAZ was calculated by subtracting the YAP/TAZ signal intensity for the cytosol from the YAP/TAZ signal intensity for the total cell. The percentage of nuclear YAP/TAZ was calculated by dividing the nuclear-localized YAP/TAZ signal by YAP/TAZ signal for the entire cell.

CRISPR/Cas9 genome editing

SpCas9 and chimeric guide RNA expression plasmid PX330 (Addgene) were used to generate stable ROR1 knockout cell lines as described (16). CRISPR targeting sequence (CCAGTGCGTGGCAACAAACGGCA) of ROR1 were designed with CRISPR Design tool (http://crispr.mit.edu/). Hs578T transfected with ROR1 CRISPR plasmids were stained for

ROR1 using 4A5-Alex647 and the ROR1-negative cells isolated and placed into culture. This process was repeated 3 successive times to isolate a population of ROR1 knock-out cells.

Immunoblot analyses

Cells used for examination of proteins via immunoblot analysis were treated with control antibody or cirmtuzumab (50 μg/ml) for overnight and then were cultured in medium supplemented with or without recombinant Wnt5a (100 ng/ml). Treated cells or tissues were lysed in buffer containing 1% NP40, 0.1% SDS, 0.5% sodium deoxylate, and protease inhibitors (Pierce). Size-separated proteins were transferred to membranes, which were incubated with primary antibodies specific for ROR1 (#4102), TAZ (#4883), YAP (#14074), pAKT(#4060S), AKT (#4691S), β-Actin (#3700, Cell Signaling Technology), BMI1 (#ab135713, Abcam), Rac1 (#ARC03), RhoA (#ARH04), cdc42 (#ACD03, Cytoskeleton), or Wnt5a (#MAB645, R&D system). After washing away unbound antibody, the membranes were incubated with secondary antibodies that were conjugated with horseradish peroxidase. Blots were prepared for enhanced chemiluminescence and autoradiography. The protein concentration was determined using a bicinchoninic acid protein assay (Pierce).

Assays for activated Rho-GTPases

RhoA and Rac1 activation assay reagents were purchased from Cytoskeleton and used according to the manufacturer's instructions. Briefly, GTP-bound active RhoA, Rac1 or cdc42 was pulled down with Rhotekin-RBD or PAK-PBD beads, respectively, and then examined via immunoblot analysis. Immunoblots of whole-cell lysates were used to assess for total RhoA, Rac1, or cdc42. The integrated optical density (IOD) of each band

was evaluated by densitometry and analyzed using Gel-Pro Analyzer 4.0 software (Media Cybernetics).

Quantitative PCR

Total RNA was extracted using Trizol (Life Technologies). A 10-μg volume of total RNA was incubated with 10 U RNase-free DNase I (Life Technologies) at 37°C for 30 minutes. RNA was purified using RNeasy (QIAGEN). The purified total RNA (2 μg) was converted to cDNA using 200 U Superscript III Reverse Transcriptase (Life Technologies). Taq 2x Master Mix (NEB) was used for PCR according to the manufacturer's protocol.

Silencing of human AKT

AKT siRNA was purchased from Cell Signaling. All siRNA transfections were performed in DMEM serum-free medium using lipofectamine RNAiMAX (Invitrogen), according to the manufacturer's instructions, and then subjected to different assays.

Statistical analyses

Unless indicated otherwise, data were presented as the mean ± standard error of the mean (SEM). Differences between two groups were determined by unpaired 2-tailed Student's t-Test. Differences between multiple groups were determined by Dunnett's multiple comparison test. All P values of less than 0.05 were considered significant. Analysis for significance was performed with GraphPad Prism 6.0 (GraphPad Software Inc.).

Sequence of primers for qPCR

GAPDH primers:	5’-GAAGGTGAAGGTCGGAGTC-3’ (forward)
	5’-GAAGATGGTGATGGGATTTC-3’ (reverse)
BMI1 primers:	5’-CGTGTATTGTTCGTTACCTGGA-3’ (forward)
	5’-TTCAGTAGTGGTCTGGTCTTGT-3’ (reverse)

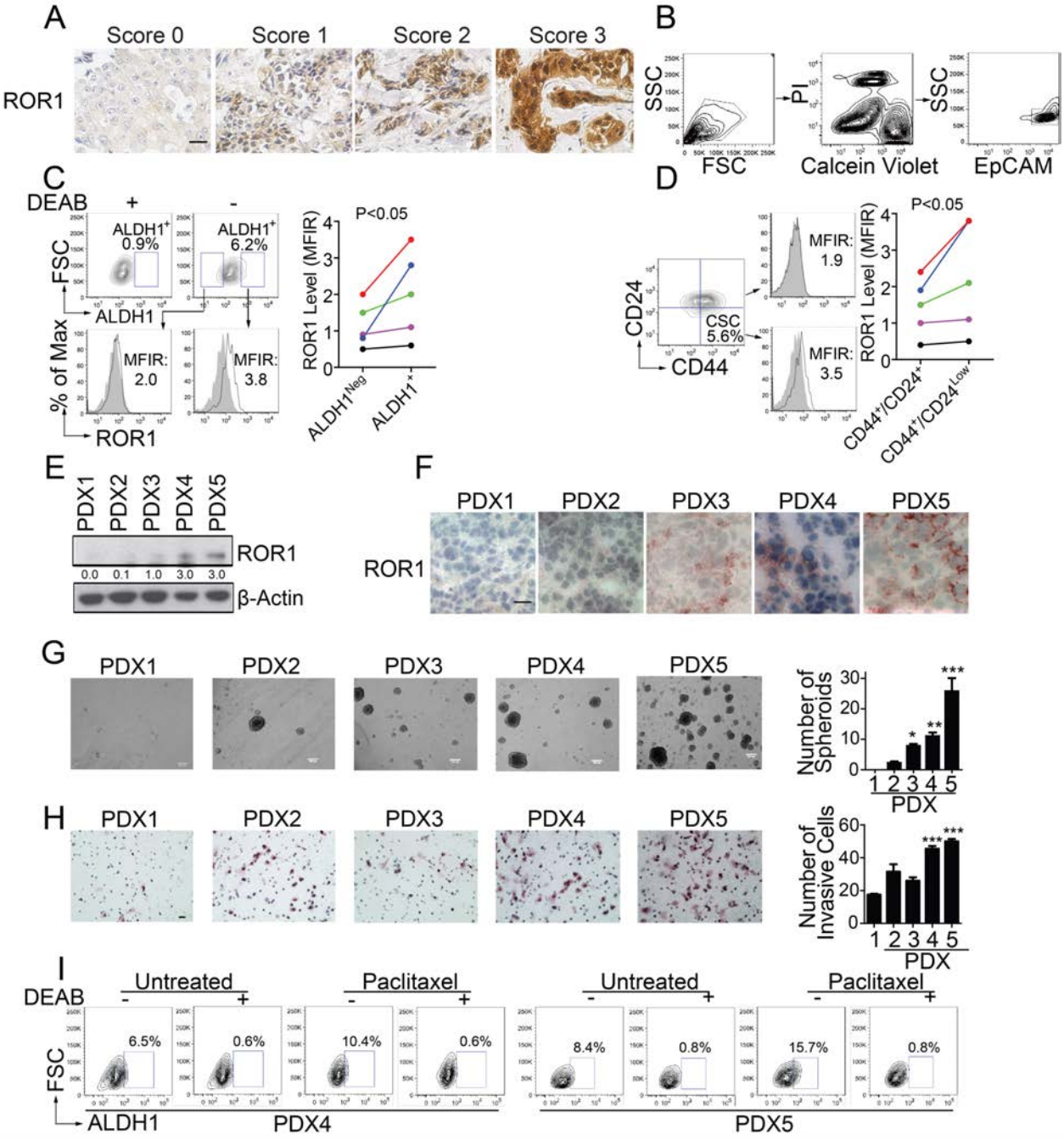

Fig. S1. ROR1^{Hi} Breast Cancers Have Enhanced Stemness Features

(*A*) Representative images of breast cancer tissues stained with the anti-ROR1 mAb, 4A5. The bound antibody is brown and the nuclear counterstain with hematoxylin is blue.

Scale bar: 25 μM. (*B*) Gating strategy for primary tumor cells isolated from each PDX. Single-cell suspensions were made from extirpated tumor nodules and stained with propidium iodide (PI), Calcein Violet or fluorescein diacetate (FDA), and fluorochrome-conjugated mAb specific for EpCAM, or an irrelevant antigen (control). We gated on cells having the appropriate forward light scatter (FSC) and side scatter (SSC) characteristics (left). We excluded dead cells labeled with PI and gated on live cells that stained with Calecein Violet (middle). Because the cells also were stained with fluorochrome-conjugated mAbs, we gated on human breast cancer cells that were stained with mAbs specific for EpCAM (right). (*C*) Cells from each PDX were stained for ROR1 with 4A5 or control mAb, and for ALDOFLUOR without (-) or with (+) the ALDH1-inhibitor, DEAB, as indicated at the top of each column of histograms. The open boxes in each contour plot in the top row indicate the gates used for defining cells with ALDH1 activity, the proportions of which are indicated. The open boxes in the left of the contour plots depict the gates used to identify cells that assuredly lacked ALDH1 activity. In the bottom row are histograms depicting the fluorescence of cells that were negative (left) or positive (right) for ALDH1 activity. The right panel provides the staining intensity for ROR1 in $ALDH1^{+}$ versus $ALDH1^{Neg}$ cells from each of the five different PDX tumors. (*D*) Cells from each PDX were stained with CD44, CD24, 4A5, or a control mAb. The histograms depict the fluorescence of gated $CD44^{+}/CD24^{Low}$ or $CD44^{+}/CD24^{+}$ cells; the shaded histograms depict the fluorescence of cells stained with an isotype-control mAb, whereas the open histograms depict the fluorescence of cells stained with 4A5. The right panel provides the ROR1 staining intensity of $CD44^{+}/CD24^{Low}$ versus $CD44^{+}/CD24^{+}$ cells from each of five different PDX. The number in each plot provides the mean fluorescence intensity ratio

(MFIR) for ROR1, which is derived from the mean fluorescence intensity (MFI) of cells labeled with the anti-ROR1 mAb divided by MFI of cells labeled with control antibody. (*E*) Lysates from each of PDX were examined for ROR1 expression via immunoblot analysis. β-Actin serves as loading control. (*F*) Tissue sections of PDX1-5 were stained with 4A5 for detection of ROR1 by IHC. Staining for bound 4A5 is in red and staining for nuclear material is in blue. Scale bar: 15 μm. (*G*) Photomicrographs of spheroids generated by cells isolated from each of PDX. Scale bar: 100 μm. The bar graph depicts the average numbers of spheroids formed by cells from each PDX in triplicate wells ± SEM. (*H*) Representative photomicrographs of invasive cells from isolated tumor cells of each PDX. To the right of the photomicrographs are bar graphs depicting the mean relative proportions of tumor cells that migrated into Matrigel (±SEM) from each tumor cell population in three independent experiments, each normalized to the proportion of the tumor cells from PDX5 that migrated into Matrigel. Scale bar: 10 μm. An asterisk represents $P < 0.05$, ** denotes $P < 0.01$, and *** represents $P < 0.001$, using Dunnett's multiple comparison test. (*I*) Single cell suspensions were generated from each PDX that were removed from PDX-engrafted mice that had not received treatment (Untreated), or had been treated with paclitaxel. We examined for ALDH1 enzymatic activity via flow cytometry. DEAB, an inhibitor of ALDH1 enzymatic activity, was used to identify cells that have ALDH1 activity. The open boxes in the right of the contour plots depict the gates used to identify cells that are certain to have ALDH1 activity. The number in each histogram depicts percentage of $ALDH1^+$ cells.

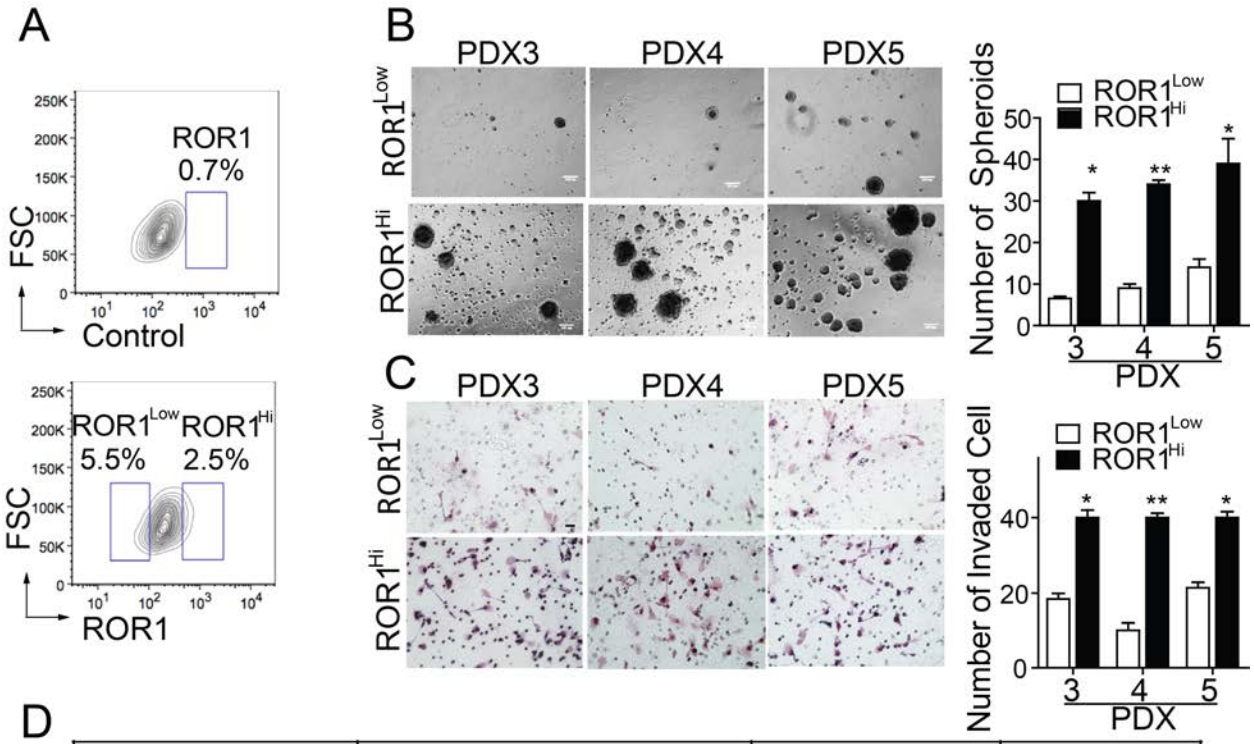

Tissue ID		Cell Number			Frequency of Tumorigenic Cell	P Value
		5000	500	100		
PDX3	$ROR1^{Low}$	0/4	0/9	0/10	1/2913	<0.01
	$ROR1^{Hi}$	2/5	5/10	1/10	Inf	
PDX4	$ROR1^{Low}$	3/6	2/6	N.D	1/455	<0.001
	$ROR1^{Hi}$	6/6	4/6	N.D	1/4740	
PDX5	$ROR1^{Low}$	N.D	1/9	0/10	1/329	<0.001
	$ROR1^{Hi}$	N.D	8/9	1/10	1/5247	

Fig. S2. $ROR1^{Hi}$ Breast Cancer Cells Have Stemness Features

(*A*) Strategy for sorting $ROR1^{Hi}$ versus $ROR1^{Low}$ cells. The open boxes indicate the gates used to select $ROR1^{Low}$ (left) or $ROR1^{Hi}$ (right) cells. (*B*) Photomicrographs of spheroids formed from $ROR1^{HI}$ or $ROR1^{Neg}$ cells isolated from each of the PDX, as indicated on the top. Scale bar: 100 μm. The bar graph to the right depicts the average numbers of spheroids formed ± SEM by each of the cell preparations in three separate cultures, as indicated at the bottom of the histograms. (*C*) Photomicrographs of Matrigel-invading cells

from ROR1^{HI} or ROR1^{Low} cells isolated from different PDX, as indicated on the top. Scale bar: 10 μm. The bar graph to the right depicts the mean invaded cells into Matrigel (±SEM) per field for 10-20 fields of each of the cell preparations in three independent experiments. (*D*) Tumor incidence in animals implanted with ROR1^{Hi} or ROR1^{Low} cells isolated from each of the various breast cancer PDX. Frequency of tumorigenic cells and probability estimates were computed using ELDA software. N.D indicates not done.

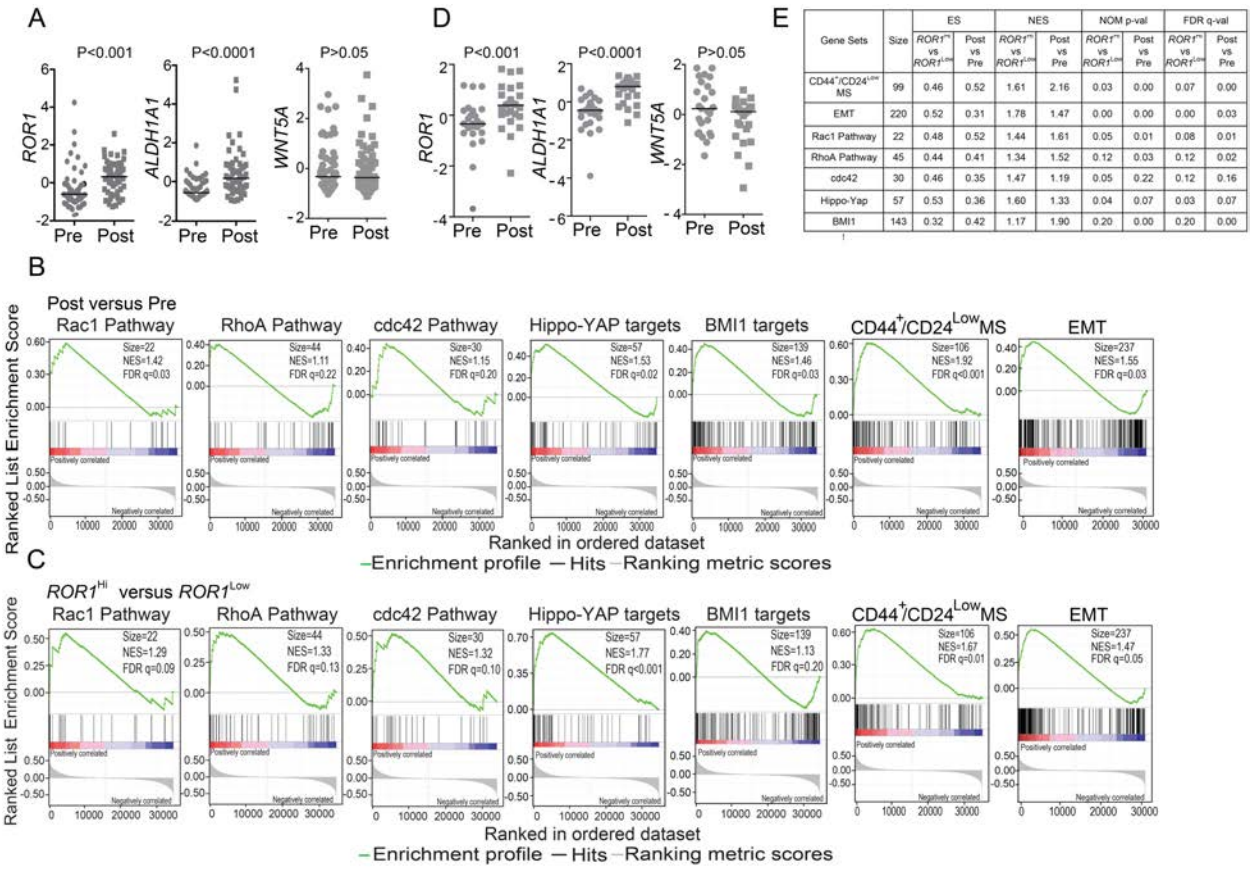

Gene Sets	Size	ES		NES		NOM p-val		FDR q-val	
		ROR1^{Hi} vs *ROR1*^{Low}	Post vs Pre	*ROR1*^{Hi} vs *ROR1*^{Low}	Post vs Pre	*ROR1*^{Hi} vs *ROR1*^{Low}	Post vs Pre	*ROR1*^{Hi} vs *ROR1*^{Low}	Post vs Pre
$CD44^{+}/CD24^{Low}$ MS	99	0.46	0.52	1.61	2.16	0.03	0.00	0.07	0.00
EMT	220	0.52	0.31	1.78	1.47	0.00	0.00	0.00	0.03
Rac1 Pathway	22	0.48	0.52	1.44	1.61	0.05	0.01	0.08	0.01
RhoA Pathway	45	0.44	0.41	1.34	1.52	0.12	0.03	0.12	0.02
cdc42	30	0.46	0.35	1.47	1.19	0.05	0.22	0.12	0.16
Hippo-Yap	57	0.53	0.36	1.60	1.33	0.04	0.07	0.03	0.07
BMI1	143	0.32	0.42	1.17	1.90	0.20	0.00	0.20	0.00

Fig. S3. Chemotherapy Can Enhance Breast Cancer Expression Of ROR1, Genes Associated With Breast Cancer Stemness

(*A*) *ROR1*, *ALDH1A1*, *Wnt5a* expression levels in matched breast cancer patient samples before ("Pre") or after chemotherapy ("Post") (Post, Pre, N=57, GSE87455). (*B*) Enrichment plots of genes activated by Rac1/RhoA/cdc42-signaling, Hippo-YAP target genes, BMI1 target genes, gene signature of $CD44^{+}/CD24^{Low}$ MS population and of gene associated with EMT on post-treatment samples (N=57) versus matched pre-treatment samples (N=57) in the GSE87455 dataset. The middle portion of the plot shows where the members of the gene set appear in the list of ranked genes; red and blue colors represent positive and negative correlation with the level of *ROR1* expression,

respectively. (*C*) Enrichment plots of genes activated by Rac1/RhoA/cdc42-signaling, Hippo-YAP target genes, BMI1 target genes, gene signature of $CD44^{+}/CD24^{Low}$ MS population and of genes associated with EMT for the *ROR1*^{Low} and *ROR1*^{Hi} sample groups from the GSE87455 (N=122). The middle portion of the plot shows where the members of the gene set appear in the list of ranked genes; red and blue colors represent positive and negative correlation with the level of *ROR1* expression, respectively. (*D*) *ROR1, ALDH1A1* or *Wnt5a* expression levels in matched breast cancer patient samples before ("Pre") or after chemotherapy ("Post") (Post, Pre, N=25, GSE21974). The line indicates the median expression level of genes in pre- versus post-treatment group. (*E*) Gene Set Enrichment (GSE) Analysis for genes associated with $CD44^{+}/CD24^{Low}$ MS, ETM, activation of Rac1/RhoA/cdc42, Hippo-YAP, BMI1 for the *ROR1*^{Low} and *ROR1*^{Hi} sample groups (N=25) or on breast cancer biopsies from patients who received neoadjuvant chemotherapy (N=25) Versus Matched Pre-treatment Samples (N=25) in the GSE21974 database. SIZE is the number of genes included in the analysis. NES (normalized enrichment score) accounts for the difference in gene-set size and can be used to compare the analysis results across gene sets. NOM p-val (nominal p value) is the statistical significance of the enrichment score not adjusted for gene set size or multiple gene sets testing, FDR q-val (false discovery rate q value) is the estimated probability that a gene set with a given NES represents a false positive. Each gene set is considered significant when the false discovery rate (FDR) is less than 0.25.

Fig. S4. Wnt5a Can Enhance Breast Cancer Expression BMI1 Protein

(*A*) *BMI1* mRNA level in Hs578T cells treated with Wnt5a at 100ng/ml at indicated time point were examined by quantitative PCR (qPCR). Data shown were the mean expression levels of *BMI1* relative to time 0 samples in triplicate and normalized with respect to GAPDH. Error bars indicate SEM. (*B*) Hs578T cells were cultured in serum-free medium, pre-treated with or without MK-2206 for 3 hours, and then stimulated with or without Wnt5a at 100ng/ml for 6 hours. BMI1, pAKT and AKT were examined on these samples via immunoblot analyses. Numbers below the row for AKT provide the ratios of band densities of pAKT to AKT that were normalized to that of samples treated for 0 minutes with Wnt5a. β-Actin served as protein-loading control. Numbers below the row for BMI1 provide the ratios of band densities of BMI1 to β-Actin, normalized with respect to that of samples treated for 0 minutes with Wnt5a.

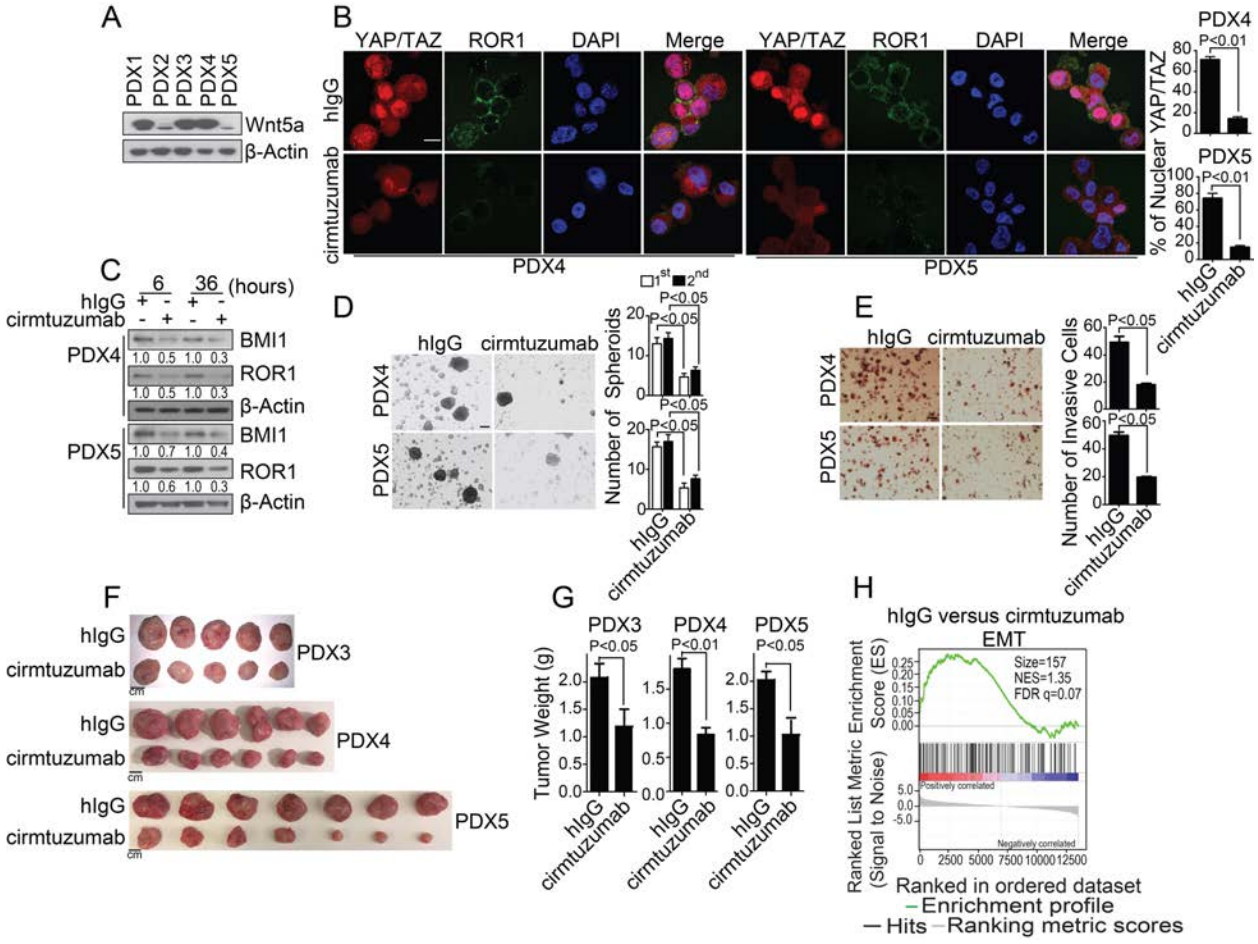

Fig. S5. Treatment With Cirmtuzumab Could Inhibit YAP/TAZ Activity And BMI1 Expression In Vitro And Repress Tumor Growth In Vivo

(*A*) Lysates from PDX1-PDX5 were examined for expression of Wnt5a, as indicated on the right margin. β-Actin serves as loading control. (*B*) Single cell suspension isolated from PDX4 or PDX5 treated with cirmtuzumab antibody or control antibody at 50 μg/ml for 4 hours were examined for YAP/TAZ via confocal microscopy. Right bar graph provides the average percentages of nuclear YAP/TAZ in the cells of each field. Scale bar: 20 μm. (*C*) Lysates from PDX4 or PDX5 treated with cirmtuzumab antibody or control antibody at 50 μg/ml for the indicated times were examined for BMI1, ROR1 or β-Actin via immunoblot analyses. (*D*) Representative photomicrographs of spheroids formed from

isolated tumor cells of different PDX treated with either control antibody or cirmtuzumab at 50 μg/ml. The bar graph on right panel depicts the average numbers of spheroids formed from tumor cells of PDX4 or PDX5 treated with cirmtuzmab or a control antibody in three separate culture wells of each treatment ± SEM. (*E*) Representative photomicrographs of invasive cells from isolated tumor cells of different PDX treated with either control antibody or cirmtuzumab at 50 μg/ml. To the right of the photomicrographs are bar graphs depicting the mean number of invaded cells of each of the cell preparations in three independent experiments ± SEM. Scale bar: 10 μm. (*F*) $1X10^6$ cells from each PDX sample in 50 μl were mixed with equal volumes of Matrigel and then injected into the mammary pad of female $Rag2^{-/-}\gamma_c^{-/-}$ mice. Tumor growth was monitored over time for 42 or 48 days. Representative photographs of each PDX removed at 42 (PDX5) or 48 (PDX4) days. Scale bar: 1 cm. (*G*) The bar graph provides average weight of tumors extirpated from the mice in each group described in figure 1A (± SEM, N=5-8). (*H*), Enrichment plots of genes associated with EMT in PDX derived from PDX4 in mice treated with control hIgG versus cirmtuzumab, as assessed via RNAseq (GSE108632).

Table S1
Clinical and Pathologic Characteristics Of Tumors From Patients Who Received Neoadjuvant Therapy

Patient Number	ER/PR/HER2 Status	Treatment	ROR1	
			Pre	Post
1	$ER^-/PR^-/HER2^+$	TEC	1	2
2	$ER^-/PR^-/HER2^-$	TE	2	3
3	$ER^-/PR^-/HER2^+$	TE	3	3
4	$ER^-/PR^-/HER2^+$	TE	1	3
5	N.D	TEC	2	2
6	N.D	TEC	2	2
7	$ER^+/PR^-/HER2^-$	TEC	2	2
8	$ER^-/PR^-/HER2^-$	TE	2	3
9	$ER^+/PR^+/HER2^-$	TAC	1	3
10	$ER^-/PR^-/HER2^-$	TE	2	3
11	$ER^+/PR^-/HER2^-$	TE	1	2
12	$ER^+/PR^+/HER2^-$	TEC	2	2
13	$ER^+/PR^+/HER2^-$	TE	2	3
14	$ER^+/PR^-/HER2^+$	TEC	3	3
15	$ER^+/PR^+/HER2^-$	TE	2	3
16	$ER^+/PR^+/HER2^-$	TEC	1	3
17	N.D	TE	1	0
18	$ER^-/PR^+/HER2^-$	TEC	2	3
19	N.D	TEC	2	3
20	$ER^+/PR^+/HER2^-$	EC	2	2
21	$ER^-/PR^-/HER2^+$	TEC	1	2
22	$ER^+/PR^+/HER2^-$	TEC	2	3

N.D: Not Defined

Table S2

Clinical, Pathologic Characteristics And Proportion Of CSCs Markers Expression Of Tumors Used To Generate Each PDX

PDX ID	ER/PR/HER2 status	Histology	P53 mutation status	Prior treatment	Expression of CSCs Markers		
					$ALDH1^+$	$CD44^+$	$CD44^+/CD24^{Low}$
PDX1	$ER^-/PR^-/HER2^+$	Ductal Carcinoma Primary Tumor	N/A	Taxane/ Platinum/ Trastuzumab	0.6%	1.8%	0.1%
PDX2	$ER^-/PR^-/HER2^-$	Ductal Carcinoma Primary Tumor	no mutations	None	2.9%	63.1%	48.8%
PDX3	$ER^-/PR^-/HER2^-$	Mixed Ductal and Lobular Carcinoma Primary Tumor	P53 mutation	Anthracycline / Taxane	3.5%	76.1%	5.6%
PDX4	$ER^-/PR^-/HER2^-$	Ductal Carcinoma Primary Tumor	P53 mutation	Taxane	6.5%	23.9%	2.3%
PDX5	$ER^+/PR^-/HER2^-$	Ductal Carcinoma Axillary Lymph Node	P53 mutation	N/A	8.4%	85.0%	6.2%

Table S3

Tumor Incidence In Animals Implanted With Different Subpopulations Of Cells Isolated From Breast Cancer PDX

Subpopulation	Cell Number		Frequency of Tumorigenic Cell	P Value
	500	100		
$CD44^{+}/CD24^{Low}$	3/4	2/4	1/265	0.002
$CD44^{+}/CD24^{+}$	0/4	0/4	1/Inf	
$ALDH1^{+}$	2/5	1/5	1/800	0.04
$ALDH1^{Neg}$	0/4	0/4	1/Inf	

$CD44^{+}/CD24^{Low}$ versus $CD44^{+}/CD24^{+}$ cells isolated from PDX4 or $ALDH1^{+}$ versus $ALDH1^{Neg}$ cells isolated from PDX5 were implanted into mammary pads of $Rag2^{-/-}\gamma_c^{-/-}$ mice (n=4-5). The numbers of mice with tumors 2 months after engraftment divided by the number of mice injected in each group are shown in the table. Frequency of tumorigenic cells and probability estimates were computed using ELDA software. Inf indicates infinite.

Table S4

Gene Set Enrichment (GSE) Analysis Of 9 Stem-Cell Gene-Expression Signatures (15) On The *ROR1*^{Hi} (N=61) Versus *ROR1*^{Low} (N=61) Samples and The *ROR1*^{Low} (N=61) Versus *ROR1*^{Hi} (N=61) Samples From Breast Cancer Patients Prior To Chemotherapy in GSE87455 Database

Gene Sets	Size	ES	NES	NOM p-val	FDR q-val
		ROR1^{Hi} vs *ROR1*^{Low}	*ROR1*^{Hi} vs *ROR1*^{Low}	*ROR1*^{Hi} vs *ROR1*^{Low}	*ROR1*^{Hi} vs *ROR1*^{Low}
Es exp1	359	0.31	0.82	0.72	0.85
Es exp2	35	-0.27	-0.71	0.87	0.97
Nanog targets*	913	0.31	1.01	0.41	0.43
Oct4 targets*	274	0.37	1.19	0.05	0.22
Sox2 targets*	678	-0.33	-1.05	0.25	0.41
NOS targets*	168	0.43	1.34	0.01	0.13
NOS TFs	37	0.55	1.40	0.06	0.10
Myc targets1	227	0.34	1.03	0.38	0.43
Myc targets2	755	-0.42	-1.28	0.04	0.14

An asterisk (*) indicates that the gene set include *ROR1.*

References

1. Martin M (2011) Cutadapt removes adapter sequences from high-throughput sequencing reads. *2011* 17(1):3.
2. Dobin A*, et al.* (2013) STAR: ultrafast universal RNA-seq aligner. *Bioinformatics* 29(1):15-21.
3. Li B & Dewey CN (2011) RSEM: accurate transcript quantification from RNA-Seq data with or without a reference genome. *BMC Bioinformatics* 12:323.
4. Yates A*, et al.* (2016) Ensembl 2016. *Nucleic Acids Res* 44(D1):D710-716.
5. Love MI, Huber W, & Anders S (2014) Moderated estimation of fold change and dispersion for RNA-seq data with DESeq2. *Genome Biol* 15(12):550.
6. Subramanian A*, et al.* (2005) Gene set enrichment analysis: a knowledge-based approach for interpreting genome-wide expression profiles. *Proc Natl Acad Sci USA* 102(43):15545-15550.
7. Kimbung S*, et al.* (2018) Assessment of early response biomarkers in relation to long-term survival in patients with HER2-negative breast cancer receiving neoadjuvant chemotherapy plus bevacizumab: Results from the Phase II PROMIX trial. *Int J Cancer* 142(3):618-628.
8. Stickeler E*, et al.* (2011) Basal-like molecular subtype and HER4 up-regulation and response to neoadjuvant chemotherapy in breast cancer. *Oncol Rep* 26(4):1037-1045.
9. Schaefer CF*, et al.* (2009) PID: the Pathway Interaction Database. *Nucleic Acids Res* 37(Database issue):D674-679.
10. Liberzon A*, et al.* (2011) Molecular signatures database (MSigDB) 3.0. *Bioinformatics* 27(12):1739-1740.
11. Fukuda T*, et al.* (2008) Antisera induced by infusions of autologous Ad-CD154-leukemia B cells identify ROR1 as an oncofetal antigen and receptor for Wnt5a. *Proc Natl Acad Sci U S A* 105(8):3047-3052.
12. Zhang S*, et al.* (2014) Ovarian cancer stem cells express ROR1, which can be targeted for anti-cancer-stem-cell therapy. *Proc Natl Acad Sci USA* 111(48):17266-17271.
13. Cui B*, et al.* (2013) Targeting ROR1 inhibits epithelial-mesenchymal transition and metastasis. *Cancer Res* 73(12):3649-3660.
14. Zhang S*, et al.* (2012) ROR1 is expressed in human breast cancer and associated with enhanced tumor-cell growth. *PLoS One* 7(3):e31127.

15. Ben-Porath I*, et al.* (2008) An embryonic stem cell-like gene expression signature in poorly differentiated aggressive human tumors. *Nat Genet* 40(5):499-507.